博士論文(要約)

FUNDAMENTAL STUDIES ON UTILIZATION OF HPC-FEM IN PRACTICAL SEISMIC RESPONSE ANALYSIS OF GROUND

(地盤工学分野の耐震設計業務における
HPC-FEM の実用化に向けた基礎的研究)

Yuichi Otsuka

大塚　悠一

Acknowledgements

First of all, I would like to express my appreciation to my committee chair Professor Muneo Hori, who has taught and mentored me since I was a bachelor student. His enthusiastic guidance, criticism and discussion were really helpful for this research. His sophisticated mathematical analysis and insight always impress and encourage me.

I also appreciate the help received from Professor Tsuyoshi Ichimura and Professor Lalith Wijerathne, who also gave a many useful help and advice in the field of computer science and mathematics. I thank them for being patient and teaching me kindle. I would also like to my gratitude to my committee members, Professor Koichi Kusunoki and Professor Kenji Watanabe for their suggestions and criticisms.

This research was carried out as a part of a research project in the Tokyo Electric Power Services Co., Ltd. I'm sincerely grateful to Dr. Yukio Tamari and many other colleagues in the company for their comments and supports which enables me to do this research.

Finally I thank my parents and sisters for their continuous supports and encouragements throughout this research.

Abstract

Finite element method (FEM), which can faithfully reproduce the shapes of structures and mechanical conditions, is widely used in engineering. In addition, with the development of computer science, a finite element method with a solver enhanced high-performance computing, namely HPC-FEM is developed.

This HPC-FEM has been introduced into the geo-tech field and three-dimensional soil-structure analysis model of a few million degrees-of-freedom, which was regarded as being difficult to solve because of the excess time required to find a solution, has been solved in recent years. This seismic response analysis with soil-structure model is essential for a seismic design in the geo-tech field. Therefore HPC-FEM is expected to increase productivity in the geo-tech field.

Seismic designs in the geo-tech fields still mainly use two-dimensional FEM, and it is rare to use three-dimensional FEM analysis models. Even if 3D FEM analysis is employed in practice, this might be a static analysis like a pushover method or a response displacement method. There is quite a gap between research and practice.

In fact, we need to improve other components of FEM for the utilization of HPC-FEM in practical geo-tech applications. Besides a solver, pre-processing for an analysis model, post-processing of numerical analysis results, and theory of the constitutive relations are important components of FEM. There are limitations not only in the solver but also in these components. We need coordinated improvement of pre-processing, solver, post-processing, and theory portions.

In this thesis, we carry out fundamental investigations to identify limitations in these components and solve the three major limitations: solver, post-processing, and theory.

First, we implement HPC-FEM technique in a existing FEM program that is used in practice. Using a validated FEM program that is used in practice reduce the initial cost for introduction of new program for a private company, so that it is important to speed up this FEM program. After the implementation, we solved some 3D FEM analysis models of underground structures, which are used in practice and showed the applicability of the CG method for practical use. The CG method was 500 times faster than the original solver.

As for the solver, we examine an ill behavior of solution in liquefaction analysis. We find that, in some analysis, a solution changes when the number of CPU cores is changed. We develop a HPC-FEM that uses quadruple precision to fix the ill behavior. This program can be a verification tool for the codes.

For the post-processing, we propose the efficient conversion method from a three-dimensional solid element model solution to a structure element model solution like a sectional force. The physical background which guarantees consistency between the solid and structure element solution is supported by meta-modeling theory. We develop the conversion method from solid element solution to Timoshenko-Beam, Mindlin Plate and shell element solution. This conversion helps engineers interpret the numerical results of a three-dimensional analysis.

For the theory of the constitutive relations, we employ a multi-spring model (MSM), which is an empirical model based on experiments and used in practice for seismic response analysis. There is a difference of solution between 2D MSM and 3D MSM in plane strain state and it causes a confusion of engineers. We do theoretical analysis of them and clarify the difference.

Contents

List of Figures

List of Tables

Chapter 1

Introduction

1.1 Background

Lower productivity compared with other engineering fields has been noticed in the field of civil engineering. A simple reason is that construction works, a major element of civil engineering production, are made in natural environment; usage of robotics and automation that are developed for manufacturing industry is difficult. It is overlooked to increase productivity for design and evaluation works which are made in office environment. Unlike other field of engineering, civil engineering constructs a unique structure at a particular site, and engineers have to design and evaluate a large number of structures. Thus, higher productivity is need for design and evaluation work.

In design and evaluation works, numerical analysis of designed structures or existing structures is an element which could contribute to higher productivity. Most of numerical analysis made in civil engineering is of smaller scale compared with other engineering fields, A critical issue is not the scale of analysis. Small-scale numerical analysis needs a large amount of human resources in preparing analysis models by suitably simplifying computer-aided design data of a structure and in interpreting analysis results by considering overestimation and approximation which are made in making the simplified model. Analyzing an analysis model of high fidelity reduces the model construction and the result interpretation, while it needs a large-scale

numerical analysis.

A large-scale numerical analysis ought to be made in an automated manner; manual handling of design data or analysis results is not feasible for an analysis model of large scale or a large amount of analysis data. Therefore, it will contribute to increase productivity if a large-scale numerical analysis that reduces required human resource is available. Utilization of such large-scale numerical analysis is a candidate to increase productivity for design and evaluation works,

A finite element method enhanced with high performance computing (referred as HPC-FEM) is a tool for realizing such large-scale numerical analysis in the geo-tech field which uses a variety of numerical analysis of seismic responses, settlement, underground water flow, bank stability, or long-term deformation of geo-tech structures [51]. HPC-FEM is being developed to have high scalability by implementing parallel computing techniques into it. A time to solution can be accurately measured for a given analysis problem and for a given computer environment. While it is currently used for research purposes of more accurate and higher resolution analysis, HPC-FEM should be utilized in practice for higher productivity.

Since FEM consists of three elements, namely, *pre-process* (constructing a set of nodes and elements), *solver* (solving a matrix equation for unknown displacement) and *post-process* (producing interpretable analysis results), we point of a major limitation for each element of HPC-FEM in utilizing it in practice. As for pre-process, however, we do not find major limitations because, in general, underground structures are not of most complicated configuration, and automated pre-processing is relatively easy[12]. Pre-processing of HPC-FEM would be more difficult when a set of man-made structures and underground structures are analyzed.

As for solver, HPC-FEM employs an iterative solver based on a conjugate gradient (CG) method, which is theoretically faster than direct solvers implemented in ordinary FEM; computation required for the CG method increases in proportion to the matrix dimension while one required for the direct solvers increases in proportion to the square of the matrix dimension. However, it is not clarified yet that the CG method actually makes a shorter time to solution for geo-tech problems; there is a possibility that the characteristics of the matrix used in the geo-tech field might not be suitable for the CG method, and the direct solver could make faster

computation up to a certain matrix dimension than the CG method.

The post-process is a weak point of HPC-FEM, because it uses numerous solid elements (the number of which exceeds 1,000,000 at least), and values at nodes or Gauss points of the solid elements must be converted to design values for a specified cross section or structural components [48]. Such conversion is time consuming when analysis results are manually handled, and greater human resources are needed as the amount of analysis results increases when a large-scale numerical analysis is made.

Besides for the three elements of FEM, we have to point out a possible bottle neck in utilizing large-scale numerical analysis of HPC-FEM in the practical geo-tech field. At this moment, most of numerical analysis of the geo-tech field is made in the two-dimensional setting. Extension from the two-dimensional setting to the three-dimensional setting is not simple since there are constitutive relations which are not easily extended to the three-dimensional setting. The extension from the two-dimensional setting to the three-dimensional setting involves a method of determining material parameters input to an analysis model from soil data which are measured in site [35].

1.2 Objective

The background mentioned in the preceding section is summarized as follows:

> Utilization of HPC-FEM in the practical geo-tech field is needed for higher productivity, and it is necessary to identify whether we can solve its major limitations.

In this thesis, we carry out fundamental studies to answer the challenge mentioned above, i.e., whether we can solve its major limitations. The goal of the utilization is to increase productivity, and hence it is not the aim of this thesis to merely import HPC-FEM which is developed in other fields of engineering in the practical geo-tech field. To realize substantial utilization, we will consider solving the three major limitations of HPC-FEM (that are summarized in the preceding section) in carrying out large-scale numerical analysis in the practical geo-tech field.

The first limitation is related to solver. HPC-FEM program and solver is already developed in research field[25, 51]. But, in practical field, engineers still use an conventional FEM program without HPC. One of the reason is that it costs a lot to introduce a new HPC-FEM program forthe companies. The companies need to show a reliability of the new program for their clients.To show a reliability, verification and validation of the new program through many numerical experiments is needed. Unlike other research which develop a new HPC-FEM program, we will implement HPC-FEM technique in an existing FEM program and enhance the program with HPC. Then companies can use HPC-FEM easily without the costs. It is literally the most fundamental step to examine the performance of the program in the geo-tech field. Once the applicability of the program is confirmed, we study the quality of large-scale numerical analysis that we are aimed.

The second limitation is related to post-processing. Engineering evaluation of underground structures is relatively easy even if a large amount of numerical results are produced; studying responses of a few points in the ground would be sufficient. Conversion must be made for man-made structures which are built on the ground. According to the meta-modeling, we are able to convert a solid element model of large degree-of-freedom to a structural element model of much fewer degree-of-freedom by satisfying the consistency with the original solid element model. We seek to develop this conversion to shell element models which are most often used in practice.

The third limitation is the extension of soil constitutive relation from the two-dimensional setting to the three-dimensional setting. In seismic design in practice, most of numerical analysis is made in the two-dimensional setting. To introduce the three-dimensional setting, comparison of two-dimensional and three-dimensional numerical analysis is needed. In this viewpoint,comparison of 2D and 3D theory of constitutive relations is beneficial. We pick up a multi-spring model, which is widely used in practice for seismic response analysis in the practical geo-tech field [23, 37, 44]. There are a few research achievements related to the difference between two-dimensional and three-dimension model through numerical experiments[24]. We do theoretical analysis of 2D and 3D MSM and clarify the differences. In addition, we propose a parameter setting method for two-dimensional settings considering this difference.

1.3 Contents

The contents of this dissertation are as follows. First, we do the literature review to examine the limitation of HPC-FEM for the utilization for practice in Chapter2. In Chapter3, we explain the strategy of this dissertation. Implementation of the CG method and HPC-FEM technique into an exisitng FEM program is explained in Chapter4. Quadruple precision in HPC-FEM is explained in Chapter5. Conversion method based on meta-modeling theory is proposed in Chapter6. Theoretical analysis of 2D and 3D multi-spring models is done in Chapter7. Concluding remarks are made in Chapter8.

Chapter 2

Literature review

Numerical Analysis in Geo-Tech field (Practice)

Numerical analysis of Geo-Tech in practice for seismic performance evaluation is mainly two dimensional analysis and the evaluation items are based on 2D analysis. For example, Atomic Energy Commission of Japan Society of Civil Engineers, JSCE, publishes the handbook of seismic performance evaluation of underground reinforce concrete structure related to Nuclear power plant[29]. In this handbook, two dimensional model of underground calvert box is shown as example case.

There a few commercial software which is capable of three-dimensional analysis in geo-tech field [11, 15, 16, 38, 40]. Most of them use direct method as a solver of matrix equation. The reason is that the direct method shows the stable performance the finite element model which is modeled by multi-materials such as soil and reinforced concrete in geo-tech field. However direct method shows low scalability in parallel computing and can solve the finite element model of less than 1,000,000 DOF in designated time.

Numerical Analysis in Geo-Tech field (Research)

In contrast,three dimensional numerical analysis are studied in research field.

Most of research considers soil-structure interaction like LNG tank [19, 45] ,pipe foundation [7, 28], Nuclear Power Plant [20, 21]. Some researches compare two-dimensional analysis and three-dimensional analysis and shows the limitation of two-dimensional one[1, 13, 42]. Some of them also use the direct solver as practice and there is the limitation of time to solution.

For the pre-process, there is movement for standardization of modeling of three-dimensional soil model in recent years[14]. Although constructing three-dimensional CAD data from geological survey depends on the engineers knowledge and couldn't be done automatically, constructing three-dimensional finite element model from CAD data can be done automatically [12]. However we should mention that this finite element model consists in quadratic tetrahedral element and its DOF it a quite large. Such a model assumes the utilization of HPC-FEM.

For the quality assurance for numerical analysis, the concept of verification and validation is being introduced into the geo-tech field in recent years[17]. For the verification of numerical analysis, numerical stable and conversion respect to mesh size and time is important.

For the post-processing, some research proposed the conversion method from solid element solution to structure element solution[26, 49]. The reason is that the seismic evaluation in practice is based on structure component like sectional force although a large scale finite element model ought to be made in automated manner with a solid element. An efficient conversion method is needed for a large scale model.

For the theory, constitutive law of soil in three-dimensional setting is often the extension of the constitutive law in one-dimensional or two-dimensional setting[50]. This extension is based on theory of Compounded Mobilized Plane, CMP, and theory of Spatially Mobilized Plane, SMP [31]. These theory is relied on the fact that stress-strain relationships of soil under three different principal stresses can uniquely be expressed by interpreting the relationships with respect to this plane [30]. A similar idea is also employed in "multi-spring model", which is often used in practical seismic design. This model consists of a multitude of non-linear 1D shear springs oriented in an arbitrary direction.on one plane. We must pay attention that two-dimensional theory is not constructed as the reduction of three-dimensional theory.

Chapter 3

Strategy of carrying out fundamental studies

3.1 Implementation of CG method and HPC-FEM technique into an existing FEM program

As the first trial, we start to implement a conjugate gradient (CG) method into a solver of an existing finite element method (FEM) program. This implementation is essential in carrying out three-dimensional FEM analysis in a designated time. Most of CPU time (or process time) is spent in solving the matrix equation or solver. Hence, a faster solver is always needed. High scalability of the solver is needed, so that time to solution can be accurately estimated for given computer environment. HPC enhancement must be added in implementing the CG method in the FEM solver.

In general, CPU time of the FEM solver increases in the linear or square promotion of the matrix dimension, respectively, when the CG solver or the direct solver is used in the FEM program; this is the major reason the CG method is employed in parallel FEM. However, there is a possibility that the direct solver has shorter time to solution for smaller scale problems. Indeed, the scale of the target problems studied here is not largest in the field of computational science. We need to quantify the speed-up of FEM when the direct solver is replaced by the CG

method and to show advantage of replacing the conventional direct solver with the CG method.

We emphasize that just replacing the solver doesn't make speed-up FEM so much. We need to implement other HPC-FEM techniques to improve parallel performance and convergence of CG method. However there is a limitation that most of FEM program used in practice in geo -tech field have a framework which compatible only serial computing, not parallel computing. Drastic change of the framework lose its program's reliability so that we need to implement HPC-FEM technique with a change of the framework as less as possible.

We implement the CG method and HPC-FEM technique into a house-made FEM program of "FLIP ROSE"; this program has been used in practice for a few decades [11]. The implementation is straightforward, together with parallelization; MPI and OpenMP directs are coded in the CG method, so that the FEM program can be executed in a wider computer environment of shared memory and distributed memory system.

Implementing the CG method, the CPU time of solving matrix equation is about 500 times faster even for the geo-tech problem. The detail is explained in Chapter 4.

3.2 Need for Coordination in Implementing HPC Development to FEM

It is surely remarkable to achieve drastic speed-up of the house-made FEM program by replacing the direct solver to the CG method, which is enhanced with MPI and OpenMP parallelization; see the preceding section. We have to note that solver is one element of the FEM program, although it consumes most of CPU time. We need to implement various modern computing techniques into other elements of FEM, in order to practically use large scale numerical computation of the three-dimensional FEM analysis.

In general, FEM consists of the following three elements: 1) pre-process of making an analysis model which consists of nodes and elements; 2) solver of solving a matrix equation for unknown nodal vector; and 3) post-processing of numerical analysis results. As for the geo-tech problem studied here, pre-processing is relatively simpler compared with other target problems

of computational mechanics, since the configuration of underground structure consists of a few layers of distinct properties and is less complicated. Improvement of solver is of essential importance; besides for the speed-up as demonstrated in the previous section, needed is the examination of the numerical stable and convergence as for the verification of the solver. The examination of the numerical stable and convergence is often overlooked in the geo-tech field. In post-process, the results of numerical analysis, which might reaches a few 10 or 100 GB depending on the scale of a problem, must be converted to engineering indices such as cross sectional force, average displacement, or pattern in deformation (dynamic modes), the size of which is a few MB at most.

In extending the numerical simulation from the two-dimensional setting to the three-dimensional setting, we have to pay attention to the limitation of the assumption of the state of plane strain. This assumption is simple, as it makes a mathematical approximation that displacement functions depend on two coordinates on a plane (or they do not depend on an out-of-plane coordinate). To rigorously derive the two-dimensional setting, we have to consider constitutive relations. Plane strain state is admissible for an isotropic material, but not necessary so for an anisotropic material; for instance, if in-plane shear strain component inducers out-of-plane stress component, the plane strain state does not hold. Figure 3.2 shows the decomposition of in-plane and out-of-plane components for an isotopically elastic material; the state of plane strain is the consequence of the mathematical approximation that displacement, strain and stress functions are independent of the out-of-plane coordinate.

In order to practically use FEM enhanced with HPC, we have to continuously implement latest HPC developments in a coordinated manner. The coordination must be taken in updating the two elements of FEM, solver and post-process, together with the theory of constitutive relations, so that the performance of HPC as a tool of numerical analysis at design state or for evaluation is *efficiently* improved. The speed-up of solver yields a larger amount of the numerical results, and the results would be useless unless proper post-processing of them are not available. While three-dimensional analysis of FEM is more appealing than two-dimensional analysis, the validity of the three-dimensional analysis depends on the validity of the employed constitutive relations; the constitutive relations have been examined in a long time for the two-dimensional analysis not for the three-dimensional analysis. Table 3.1 summarizes the present limitations of

the three elements of FEM and theory.

	Limitation	Solution
pre-process	model geometry construction	automated meshing
	parameter determination	collaboration with experiment
	validation of analysis model	coordination with in-site measurement
solver	applicability	examination of CG method
	verification of code	examination of numerical convergence
	scalability	tune-up of solver, development of new algorithm
post-process	estimation of engineering index	conversion among consistent models
	visualization	usage and development of software/hardware
theory	extension from 2D to 3D	theoretical analysis
	numerical stability	theoretical analysis
	uncertainty quantification	usage of capacity computing

Table 3.1: Limitation and Solution of

3D	2D ($u_{i,3}(x_1,x_2)=0, \sigma_{ij,3}(x_1,x_2)=0$)	
	In-plane	Out-of-plane
$\boldsymbol{\epsilon} = \text{sym}\boldsymbol{\nabla u}$ $\epsilon_{ij}(x_1,x_2,x_3) = \frac{1}{2}(u_{i,j}(x_1,x_2,x_3) + u_{j,i}(x_1,x_2,x_3))$	$\epsilon_{11}(x_1,x_2) = u_{1,1}(x_1,x_2)$ $\epsilon_{22}(x_1,x_2) = u_{2,2}(x_1,x_2)$ $\epsilon_{12}(x_1,x_2) = \frac{1}{2}(u_{1,2}(x_1,x_2) + u_{2,1}(x_1,x_2))$	$\epsilon_{31}(x_1,x_2) = \frac{1}{2}u_{3,1}(x_1,x_2)$ $\epsilon_{32}(x_1,x_2) = \frac{1}{2}u_{3,2}(x_1,x_2)$
$\boldsymbol{\nabla}\cdot\boldsymbol{\sigma}=\boldsymbol{0}$ $\sigma_{ij}(x_1,x_2,x_3) = C_{ijkl}\,\epsilon_{kl}(x_1,x_2,x_3$	$\sigma_{11,1}(x_1,x_2)+\sigma_{21,2}(x_1,x_2)=0$ $\sigma_{12,1}(x_1,x_2)+\sigma_{22,2}(x_1,x_2)=0$	$\sigma_{31,1}(x_1,x_2)+\sigma_{32,2}(x_1,x_2)=0$
$\boldsymbol{\sigma}=\boldsymbol{C}:\boldsymbol{\epsilon}$ $\sigma_{ij}(x_1,x_2,x_3) = C_{ijkl}\,\epsilon_{kl}(x_1,x_2)$	$\sigma_{11}(x_1,x_2) = C_{11ii}\,\epsilon_{ii}(x_1,x_2)$ $\sigma_{22}(x_1,x_2) = C_{22ii}\,\epsilon_{ii}(x_1,x_2)$ $\sigma_{12}(x_1,x_2) = 2\,C_{1212}\,\epsilon_{12}(x_1,x_2)$ (i = 1,2)	$\sigma_{31}(x_1,x_2) = C_{3131}\,\epsilon_{31}(x_1,x_2)$ $\sigma_{32}(x_1,x_2) = C_{3232}\,\epsilon_{32}(x_1,x_2)$

Table 3.2: Decomposition of In-Plane and Out-of-Plane Components for Isotopically Elastic Material

3.3 Strategy of Coordinated Improvement

At this moment, the use of the three-dimensional FEM analysis is limited in practice. This is mainly because the three-dimensional FEM analysis has not been matured; it was a few years ago that an analysis model of a few million degree-of-freedom could be solved within an acceptable time to solution, by using a large scale parallel computer. Thus, the reliability of the three-dimensional FEM analysis is inevitably questioned.

The first step to realize the three-dimensional FEM analysis is to assure the reliability, and the fundamental studies for this purpose are the examination of the numerical stable (solver) and the validation of extending the two-dimensional constitutive relation to the three dimensional setting (theory). The practical usefulness of the three-dimensional analysis is demonstrated, as well, and suitable post-processing has to be developed as the fundamental study.

As for solver, we first examine the numerical stable of the CG method; it uses numerical tolerance for the numerical convergence, which make an ill behavior of solution. It means that solution changes when the number of CPU cores is changed. We develop a HPC-FEM that uses quadruple precision to fix the ill behavior.

As for post-process, we apply the meta-modeling theory[22] according to which numerical results of a three-dimensional solid element model can be ruinously converted to a frame element model such as truss element or beam element. Shell elements are most often used in practice, due to its high accuracy. We study the conversion of a solution of a solid element model to a solution of the corresponding shell element model. Unlike previous works for truss or shell element (which uses ordinary a Cartesian coordinate system)[26], we have to rigorously formulate the convergence by using a suitable general curved coordinate system that is relevant to the geometrical configuration of shell.

As for the constitutive relations that are used in practical geo-technical engineering, we employ *multi-spring model*[23, 24, 44], MSM, which is an empirical model based on experiments. We do theoretical analysis of two-dimensional and three-dimensional MSM and clarify the difference of two-dimensional MSM. The extension of this model from the two-dimensional setting to the three-dimensional setting is not completed. Unlike preceding studies, we consider reversely, i.e., the reduction from the thee-dimensional setting to the two-dimensional setting, in order to clarify the limitation of the reduction; while the extension from the two-dimensional setting to the three-dimensional setting can be made in an intuitive manner, the reduction from the three-dimensional setting to the two-dimensional can be made most rigorously.

Chapter 4

Implementation of HPC-FEM technique into an existing FEM program

4.1 Introduction

In the field of computer science and computational science, HPC (High Performance Computing) with a large-scale parallel computer is being developed. HPC is applied to various fields and, in geo-tech engineering, there is a research about numerical experiments with HPC[51]. For example, a fine element method enhanced with HPC, HPC-FEM, can do seismic response analysis of three dimensional FEM model of soil with a few billion DOF (degree of freedom)[25].

On the other hand, in practical seismic design of geo-tech field, companies still use two dimensional analysis with FEM models of several tens of thousands. And they use not a HPC-FEM program, but a conventional FEM program which uses a serial computing. In geo-tech field, there is a large gap in the use of HPC-FEM between research and company.

One of the reason of this gap is that it costs a lot to introduce a new HPC-FEM program for the companies. The companies need to show a reliability of the new program for their clients. To show a reliability, verification and validation of the new program through many numerical experiments is needed.

In addition, the companies need to have a parallel computer. Unlike research organization, one medium company is not afford a large-scale parallel computer. And the companies need to hire a professional who can deal with the computer. Such a cost is also a one of the reason of the gap.

With this background, our research studies on the utilization of a HPC-FEM in practical seismic response analysis. For the utilization, unlike other research which develop a new HPC-FEM program, we try to enhance an existing FEM program which has been used in practice to HPC-FEM. Speed-up the FEM program which has already a reliability can reduce the introducing cost and enable the companies to use HPC-FEM in practice.

We explain a strategy of improving the program. Changing the source code of the program drastically loses the program's reliability. So we minimize the modification of the source code and don't change the structure of subroutines in the program. With this strategy, we try to speed-up the program.

The contents of this chapter are as follows. First we explain the parallel computer which is used in this research and mention a possibility of cloud computing to prepare a large-scale parallel computers in practice in Section 4.2. In Section 4.3, we show the target FEM program in this study and explain the govering equation and the procedures of this program. Parallel assembling of matrix and vector are explained in section 4.4. Implementation of a conjugate gradient method in a solver is explained in Section 4.5. Comparison with the original program and the upgraded program is shown in Section 4.6. In Section 4.7, we did the numerical experiments and examine the performance of the upgraded program.

4.2 Parallel computing machine

Companies need to procure a parallel computer to use HPC-FEM There are various kinds of parallel computers and parallel computing and we need to select an appropriate one for our objective. In this section, we select the appropriate one.

4.2.1 OpenMP and MPI

OpenMP and MPI are important concepts of parallel computing.

OpenMP is a intra-node parallelization in a shared memory computer. In a share memory computer, each processors has shared memory space. OpenMP defines compiler directives and environment values for the parallelization. All you have to do is to put the compiler directives on each loop of operations for the parallelization. We don't need to modify the original codes so much.

MPI (Message Passing Interface) is a inter-node parallelization in a distributed memory computer. In a distributed memory computer, each processors has independent memory space. There are many "node", which is a pair of processor and memory and they are connected with InfiniBand or Ethernet. When one node needs to use data on other node's memory, data transfer between nodes is needed. MPI defines libraries for the data transfer. We need to write explicit instructions for the parallelization. In addition, we need to allocate data to each nodes appropriately to reduce data transfer and get a good scalability of the the parallelization. So that we need to modify the original codes much.

As we discussed in Sec 4.1, we need to minimized the modification of the original codes. In this viewpoint, penMP is preferable to MPI..

4.2.2 On-premise and Cloud computing

Companies need to procure a parallel computer to use HPC-FEM. They are two ways for it. One is to own a parallel computer (On-premise) and the other is to use a cloud computing.

When companies own a parallel computer, they need to pay not only initial costs but also maintenance costs. Unlike research organizations which use computer machines all the time, the demand of computer machines in companies is not the same and changes with order business. This demand is usually small, but once the business is ordered, companies need a large amount of computing machines. The least amount of computer machine is needed to develop and verify a program, but it is impractical to have a large amount of one to deal with

the temporal demand.

On the other hand, recently HPC using a cloud computing has attracted a lot of attention [2, 18, 32, 39]. A cloud computing is a service using an application and computer machine at a remote facility through the internet[33]. AWS EC2[5] presented by Amazon and Microsoft Azure[6] presented by Microsoft are famouse one. Companies can use computer machines as many as they need in a certain period so that they can deal with the change of demand of computer machines. They don't have to have own computer machines and reduce the initial and maintenance costs.

Some research shows that the performance of a communication between nodes by MPI in a cloud computing is worse that in an actual hardware and scalability of MPI is not good[2, 18]. On the other hand, OpenMP, which doesn't do communication between nodes shows the same scalability in a cloud computing as in an actual hardware. In this viewpoint, OpenMP is preferable to MPI.

4.2.3 Computer in this research

As we discussed, OpenMP is preferable to MPI for our objective so that we select OpenMP and shared memory computer. Table 4.1 shows the detailed of the computer in this research. It contains four processors and 64 cores and has non-uniform memory access(NUMA) memory architecture.

Table 4.1: CPU and Memory (1 socket)

CPU	Frequency	# of cores	FLOPS
Xeon E5-4660 v4	2.20 GHz	16	563.2 GFLOPS

Memory	Max Memory Bandwidth	Cashe
DDR4	63.58 Gib/s	L1: 512 KiB/core, L2: 4 MiB/core, L3: 40 MiB/socket

4.3 Problem Settings

In this section, we explain the target FEM program and select subroutines to speed-up.

We implement a HPC-FEM into an existing FEM program of "FLIP ROSE"[11], which has been used in practice for a few decades. In practice, FLIP ROSE 2D , which is a program for two dimensional analysis is often used , but FLIP ROSE 3D, which is a program for three dimensional analysis is seldom used because of too long time to solution. An extreme example, in past analysis, is that used about 32 days for a 40,000 time steps for a model of 28,000 DOF[9].

FLIP ROSE 3D is a non-linear dynamic effective stress analysis program and uses a FEM model of soil and structures. A governing equation is shown in Eq.(4.1). The equation is discretized spatially with fine elements and temporally with Newmark-method ($\beta = 0.25$).

$$\mathbf{A}\delta\mathbf{u}^{(n)} = \mathbf{b}, \tag{4.1}$$

where

$$\mathbf{A} = \frac{4}{\mathrm{d}t^2}\mathbf{M} + \frac{4}{\mathrm{d}t^2}\mathbf{C}^{(n-1)} + \mathbf{K}^{(n-1)},$$
$$\mathbf{b} = \mathbf{F}^{(n)} - \mathbf{Q}^{(n-1)} + \mathbf{C}^{(n-1)}\mathbf{v}^{(n-1)} + \mathbf{M}\left(\mathbf{a}^{(n-1)} + \frac{4}{\mathrm{d}t}\mathbf{v}^{(n-1)}\right),$$

$\mathrm{d}t$ is an increment of time step and n is time step. $\delta\mathbf{u}, \mathbf{v}, \mathbf{a}$ are displacement vector in increment form, velocity vector and acceleration vector. $\mathbf{F}, \mathbf{Q}$ are outer force vector and inner force vector. $\mathbf{M}, \mathbf{C}, \mathbf{K}$ are mass matrix, damping matrix and stiffness matrix (We use Rayleigh damping matrix). $\mathbf{K}$ and $\mathbf{Q}$ are computed with a constitutive law of each elements. FLIP ROSE 3D uses a multi-spring model[24, 44] for a constitutive law of soil and uses pore water pressure model[23] for liquefaction in undrained case. And structure elements like beam and plate are used for structures.

FLIP ROSE 3D do these procedures below at each time step.

1. Compute the coefficient matrix $\mathbf{A}$
2. Compute right-hand side vector $\mathbf{b}$
3. Solve the equation, $\mathbf{A}\delta\mathbf{u}^{(n)} = \mathbf{b}$ and yield $\delta\mathbf{u}$
4. Update $\mathbf{u}, \mathbf{v}, \mathbf{a}$ with $\delta\mathbf{u}$
5. Update state variable of elements

6. Update time step n and return 1.

.

Table 4.2 shows the CPU time of these procedures. Solver of the equation takes much CPU time and CPU time of procedures 1. and 2, are not negligible. In this research, we try to speed up these three procedures.

Table 4.2: CPU Time of the procedures

Computation of **A**	Computation of **b**	Solver of the equation
196 (s)	72 (s)	3200 (s)

4.4 Parallelization of assembling matrix and vector (closed information)

4.5 Implementation of CG method into solver (closed information)

4.5.1 CG method

4.5.2 Precondtioning matrix

4.6 HPC FLIP ROSE 3D (closed information)

4.7 Numerical Experiments

We did numerical tests of seismic response analysis and examined the performance of the CG method compared with the direct solver for matrix equations of the geo-tech field. We prepared there FEM models as follows; a) soil with horizontal layers, b) soil with a pile foundation, c) soil with a underground structure. All models have liquefaction layers.

4.7.1 Soil with horizontal layers (Case A)

The FEM model of soil with horizontal layers is shown in Fig. 4.1. The DOF of this model is about 3,000,000. Table4.3 shows the parameters of the layers. Only layer 4 is a liquefaction layer. Fig.4.2 shows the input ground motion. Time increment, dt, is 0.01 (s) and the number of time step is 2,000.

Table 4.4 shows the CPU time. We compare three programs: 1) Original program, 2)Program with direct solver, MUMPS[4, 3], which is often used as direct solver 3) Program with the HPC-FEM technique. CG method is more than 40 times faster than direct method. Total computational time of this analysis is just one day and 7 hours.

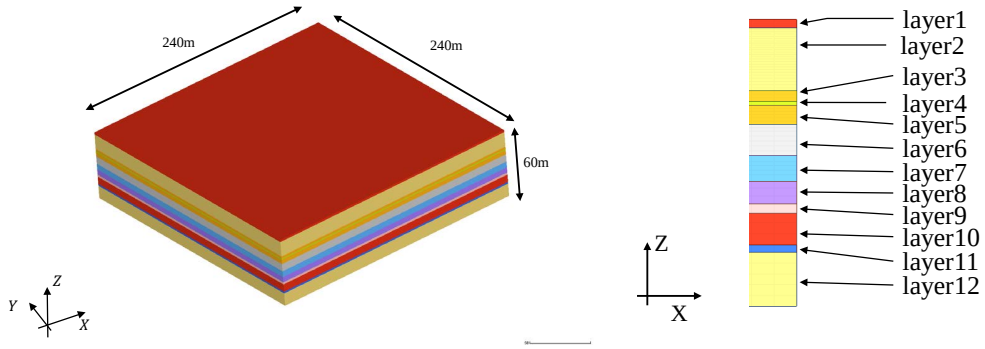

[1] soil [2] soil layer

Figure 4.1: FEM model of soil with horizontal layers

Table 4.3: input parameter for soil

	ρ (t/m^3)	Vs (m/s)	G_{ma} (kPA)	ϕ_f (deg)	h_{max}	
layer 1	1.90	152	45000	43.0	0.24	-
layer 2	1.90	152	45000	43.0	0.24	-
layer 3	2.00	180	62000	35.0	0.24	-
layer 4	1.80	180	62000	43.0	0.24	liquefaction layer
layer 5	1.80	178	57000	43.0	0.24	-
layer 6	1.90	215	88000	43.0	0.24	-
layer 7	1.90	206	81000	43.0	0.24	-
layer 8	1.90	262	130000	43.0	0.24	-
layer 9	1.90	256	125000	43.0	0.24	-
layer 10	1.90	262	130000	43.0	0.24	-
layer 11	1.70	251	120000	43.0	0.24	-
layer 12	1.90	390	290000	43.0	0.24	-

ρ: density; Vs: shear wave velocity; G_{ma}: elastic shear modulus at a confining pressure; ϕ_f: shear resistance angle; h_{max}: damping

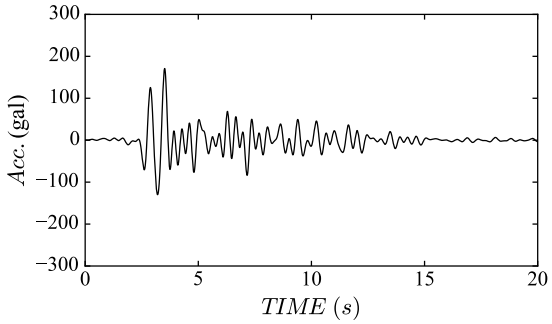

[1] x-direction

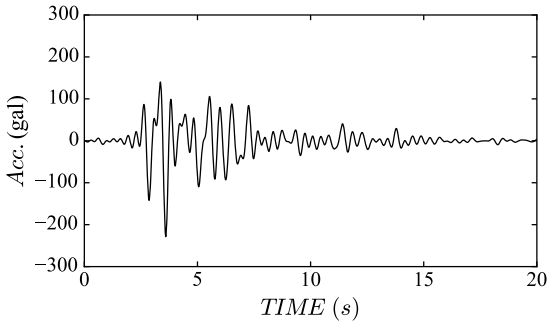

[2] y-direction

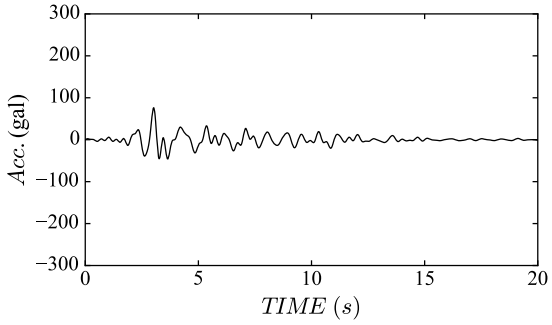

[3] z-direction

Figure 4.2: Input ground motion

Table 4.4: CPU time
(number of CPU cores is 64)

	FLIP ROSE 3D	FLIP ROSE 3D with MUMPS	HPC FLIP ROSE 3D
Solving matrix equation	3200 (s)	346 (s)	7.9 (s)
Assembling global matrix	196 (s)	196 (s)	4.7 (s)
Assembling global vector	72 (s)	72 (s)	3.2 (s)
Total analysis	-	40 days	1 day and 7 hours

4.7.2 Soil with pile foundation (Case B)

Next we did a seismic response analysis with the FEM model of soil with the pile foundation. Shapes and material properties are shown in Fig. 4.3,4.4 and Table 4.5,4.6. Only layer 4 of soil is a liquefaction layer. The pile foundation is modeled with linear solid elements and linear beam elements. The DOF of this model is about 60,000. Input ground motion is shown in Fig. 4.2.

Table 4.7 shows the cpu time to solve the equation. The CG method was more than 3 times faster than the direct method, MUMPS.

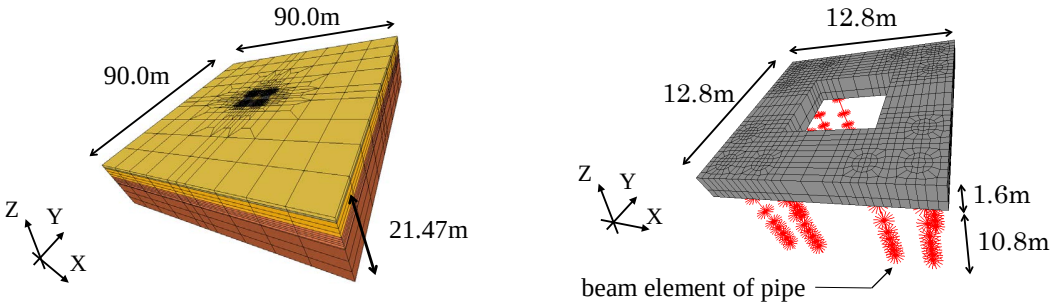

[1] soil [2] pile foundation

Figure 4.3: FEM model of soil with pile foundation

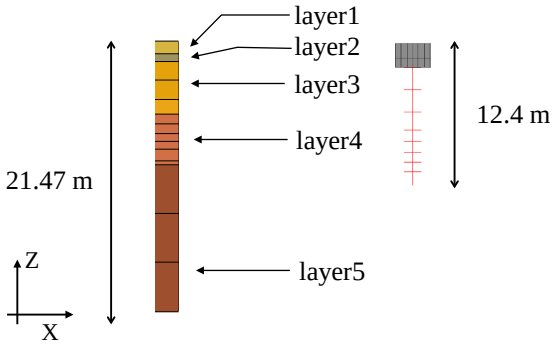

Figure 4.4: Soil layer

Table 4.5: material parameters for soil

	ρ (t/m^3)	Vs (m/s)	G_{ma} (kPA)	ϕ_f (deg)	h_{max}	
layer 1	1.60	132	28000	39.0	0.24	-
layer 2	1.70	132	28000	38.8	0.24	-
layer 3	2.00	245	120000	43.9	0.24	-
layer 4	1.90	190	69000	40.0	0.24	liquefaction layer
layer 5	2.10	351	260000	43.8	0.24	-

ρ: density; Vs: shear wave velocity; G_{ma}: elastic shear modulus at a confining pressure; ϕ_f: shear resistance angle; h_{max}: damping

Table 4.6: material parameters for foundation

ρ (t/m^3)	f (N/mm^2)	E (kPA)	G (kPA)	ν
2.50	24	2.50×10^7	1.04×10^7	0.2

ρ: density; f: compressive strength of concrete;
E: young's modulus; G: elastic shear modulus; ν: poisons ratio

Table 4.7: CPU time of solver
(number of CPU cores is 64)

direct method (MUMPS)	CG method
1.9 (s)	0.5 (s)

4.7.3 Soil with underground structure (Case C)

Finally we did a seismic response analysis with the FEM model of soil with the underground cylindrical structure.

FEM model

Fig.4.5 shows the FEM model. There are 7 horizontal layers of soil. The material properties of the layers are shown in Table 4.8. Elastic beam and shell element are used for underground cylindrical structure. The material properties of the structure are shown in Table 4.9. There is concentrated force at the center of the shell. We regard the shell element as a rigid one to resist this force so that stiffness of the shell element is more than 100 times than that of the beam element. The DOF of this model is about 1,800,000.

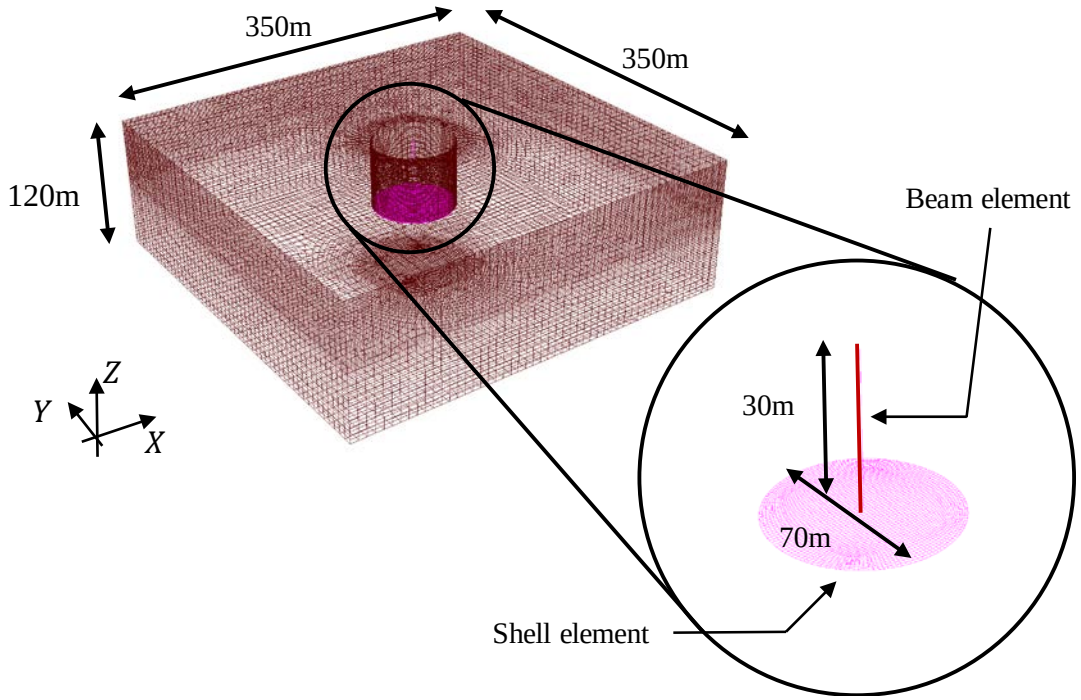

Figure 4.5: FEM model of the soil with underground structure

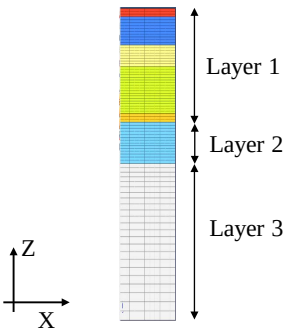

Figure 4.6: soil layer

Table 4.8: input parameter for soil

	ρ (t/m^3)	Vs (m/s)	G_{ma} (kPA)	ϕ_f (deg)	h_{max}	
layer 1	1.90	160-300	50000-20000	39-44	0.24	liquefiable layer
layer 2	1.90	470	420000	45	0.24	liquefiable layer
layer 3	1.70	550	480000	45	0.24	-

ρ: density; Vs: shear wave velocity; G_{ma}: elastic shear modulus at a confining pressure; ϕ_f: shear resistance angle; h_{max}: damping

Table 4.9: material parameters for a structure

	ρ (t/m^3)	f (N/mm^2)	E (kPA)	G (kPA)	ν
beam element	2.50	24	2.50×10^7	1.04×10^7	0.2
shell element	2.50	24	2.50×10^9	1.04×10^9	0.2

ρ: density; f: compressive strength of concrete;
E: young's modulus; G: elastic shear modulus; ν: poisons ratio

target structure for preprocess matrix

In this case, the stiffness of the structure element is very rigid so that the convergence of the CG method might be bad. Therefore we use the preprocess matrix of Eq. 4.7. We set three case of target structures for $\mathbf{A}_{SS}$ (see Table 4.10). Case A means that we use a diagonal scaling for preprocess matrix.

Table 4.11 shows the cpu time of calculating inverse matrix of $\mathbf{A}_{SS}$. It takes a lot of time, but the structures are elastic so that we have to compute only once.

Table 4.10: target structures for preprocess matrix

Matrix A	Matrix B	Matrix C
none	beam	beam+shell

Table 4.11: CPU time of inversion of matrix of $\mathbf{A}_{SS}$

Matrix A	Matrix B	Matrix C
0.0 (s)	0.01 (s)	888 (s)

static analysis

Before the dynamic analysis, static analysis is conducted by gravity in order to simulate the initial stress of soil and section force in structures.

Horizontal displacement is fixed at side surface of soil and structures and both horizontal and vertical displacement is fixed at the base through static analysis. In addition, vertical displacement of all nodes of the shell is same to avoid stress concentration at the center of shell (See Fig. 4.7).

Table 4.12 shows the computational time of solver in the static analysis. The fastest case is Case A which use a diagonal scaling for preprocess matrix. Case A is more than 10 times faster than direct method. Case B is slower than Case A and Case C is not converged.

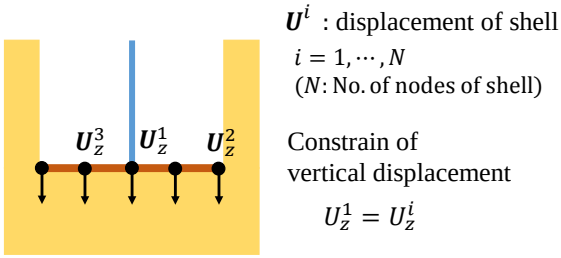

Figure 4.7: constrain of vertical displacement of shell

Table 4.12: CPU time of solver in static analysis
(number of CPU cores is 64)

direct method (MUMPS)	CG method (Matrix A)	CG method (Matrix B)	CG method (Matrix C)
175 (s)	15.9 (s)	18.07 (s)	not convergence

dynamic analysis

With the initial conditions, an dynamic analysis is conducted. Input ground motion is shown in Fig. 4.8.

We set a viscous boundary at side surface of soil and at base. In addition, we set constrain of

horizontal displacement between structures and the surrounding soil (See Fig.4.9). We should mention that there is no constrain related to vertical displacement so that structure can be slipped vertically.

Table 4.13 shows the CPU time of solver in the dynamic analysis. The fastest case is Case C which was more than 50 times faster than the direct method, MUMPs.

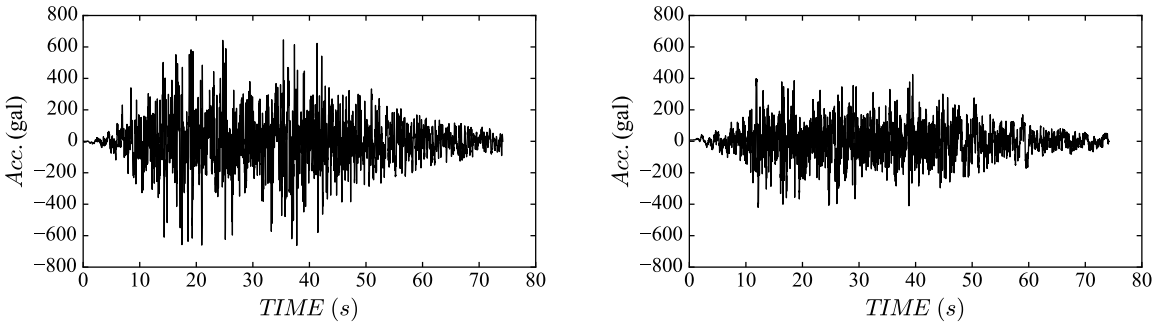

[1] x-direction [2] z-direction

Figure 4.8: Input acceleration

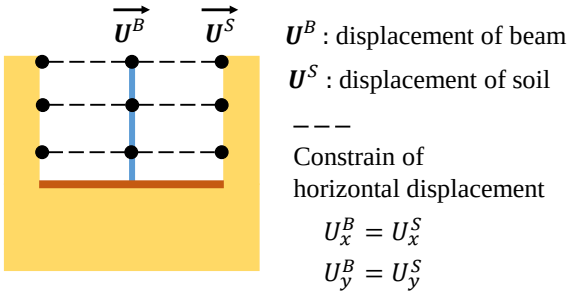

Figure 4.9: constrain of horizontal displacement

Table 4.13: CPU time of solver in dynamic analysis
(number of CPU cores is 64)

direct method (MUMPS)	CG method (Matrix A)	CG method (Matrix B)	CG method (Matrix C)
224 (s)	57.1 (s)	58.0 (s)	4.2 (s)

4.7.4 Discussions

We discuess the results of the numerical experiments. Table 4.14 shows the CPU time of all numerical tests. In all cases, the CG method is faster than the direct method. Especially the CG method shows a better performance with more than 1,000,000 DOF FEM model.

As we expect, the CG method shows a bad convergence with a FEM model which consists in rigid structure elements, but we are able to improve it with the appropriate preprocess matrix. And we find that convergence of the CG method changes with constrain condition too. We should chose an appropriate preprocess matrix considering not only material properties but also constrain conditions.

Table 4.14: CPU time of solver
(number of CPU cores is 64)

	direct method (MUMPS)	CG method
Case A (3,000,000 DOF, Dynamic)	346 (s)	7.9 (s)
Case B (60,000 DOF, Dynamic)	1.9 (s)	0.5 (s)
Case C (1,800,000 DOF, Static)	175 (s)	15.9 (s)
Case C (1,800,000 DOF, Dynamic)	224 (s)	4.2 (s)

4.8 Conclusion

In this chapter, for the utilization of a HPC-FEM in practical seismic response analysis in geo-tech field, we try to enhance an existing FEM program which has been used in practice with HPC-FEM and speed-up it. And we did the numerical experiments with the three FEM model of soil and structure and examined the performance of the program. Our solver is 500 times faster than the original one and the program used only about one day for the FEM model of 3 million DOF and 2,000 time steps. The propose method minimizes the modification of the original source code to sustain the reliability of the original program and uses a shared memory computer which can be easily used by a cloud computing. So the proposed method is expected to enable companies in the geo-tech field enhance their own FEM program with HPC easily and reduce the introducing cost of HPC-FEM program which is regraded as the one of the limitation of using HPC-FEM in practice.

Chapter 5

Implementation of quadruple precision in HPC-FEM

5.1 Introduction

After the implementation of HPC-FEM technique, we found an ill behavior of the solution of the analysis of the soil with the underground structure which was shown in Chapter 4. The ill behaviour means that a solution changes when the number of cores is changed. We need to fix this ill behavior to clarify the verification of the code.

The difference of the solution happened mainly at the interface between tje soil and the structure. In practical geo-technical engineering, we often use a FEM model with solid elements for soil and structure elements for a structure. There can be a large difference of stiffness between soil and structure, especially when soil is liquefied. This difference makes numerical errors, such as rounding errors. Usually these errors are small and we can ignore them. But with FEM model which consists in liquefaction soil whose stiffness can decline by 1 % and very rigid structures, the difference of stiffness is a quite large and can makes the ill behavior of the solution.

Using high precision computation is a one of the method to reduce numerical errors. We implement a quadruple precision into the CG method and the forming global matrix and vector

so that most of numerical errors are suppressed. We use HPC-FEM with a quadruple precision as a verification tool of the codes.

After the implementation, we did the numerical tests with three FEM models to check whether HPC-FEM with a quadruple precision can fix the ill behavior.

This contents of this chapter are as follows. First we show the ill behavior of the solution of the analysis of the soil with the underground structure. And the implementation of quadruple precision in the CG method and the forming global matrix and vector are explained in Section 5.3 and Section 5.4. Then, in Section 5.5, we did the numerical tests of seismic response analysis with three FEM models in double and quadruple precision and examine the ill behavior of the solution.

5.2 Ill behavior of solution

In this section, we show the ill behavior the ill behavior of the solution of the analysis of the soil with the underground structure which was shown in Chapter 4. The ill behaviour means that a solution changes when the number of cores is changed.

First of all, We define a difference of a solution by displacement of nodes as follows,

$$\text{Difference} = max|u_{64}^{(i)} - u_{32}^{(i)}| \tag{5.1}$$

where

$u_{64}^{(i)}$: i-th nodal displacement when the number of CPU cores is 64

$u_{32}^{(i)}$: i-th nodal displacement when the number of CPU cores is 64

Fig. 5.1 shows time history of the difference and it started to increase at around 40 (s). Fig. 5.2 shows the difference at 74.4 (s) when input ground motion is finished. The difference is local and occurs near the interface between the soil and the structure.

We set an evaluation point where the difference gets maximum value at 74.4 (s) (see Fig. 5.2). Fig. 5.3 shows the time history of displacement at the evaluation point. There is a difference only

in z-direction. A displacement in x-direction at the interface is constrained with a displacement of elastic beam elements. On the other hand, a displacement in z-direction at the evaluation point is not constrained. This slippage interface might effect the ill behavior. Fig.5.4 shows the time history of pore water pressure ration, in other words, ratio of effective stress decrease, 1-σ'_m/σ'_{m0}, near the evaluation point. There is also a difference from 38(s).

We also calculate shear stiffness, k, of liquefaction layers of soil and structures. Shear stiffness is calculated with shear modules, G, and surface area, A.

$$k = GA \tag{5.2}$$

Shear modules of soil is calculated as follows.

$$G = G_{ma}\sqrt{\sigma'_m/\sigma'_{m0}} \tag{5.3}$$

where σ'_m is effective stress and σ'_{m0} is initial effective stress. σ'_m decreases with liquefaction. Table 5.1 shows the beam element and the soil near the evaluation point. The Shear stiffness of the beam element is 10^7 times than that of the soil A large difference of stiffness of soil and structures might make numerical errors and the ill behavior.

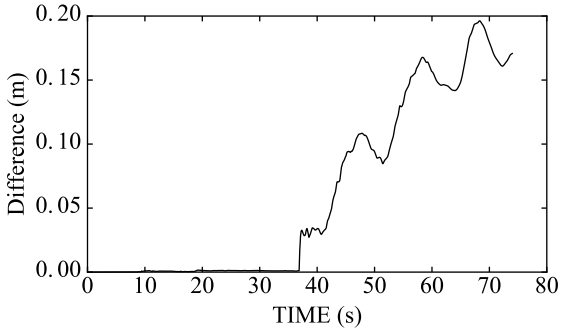

Figure 5.1: Time history of the difference of the displacement

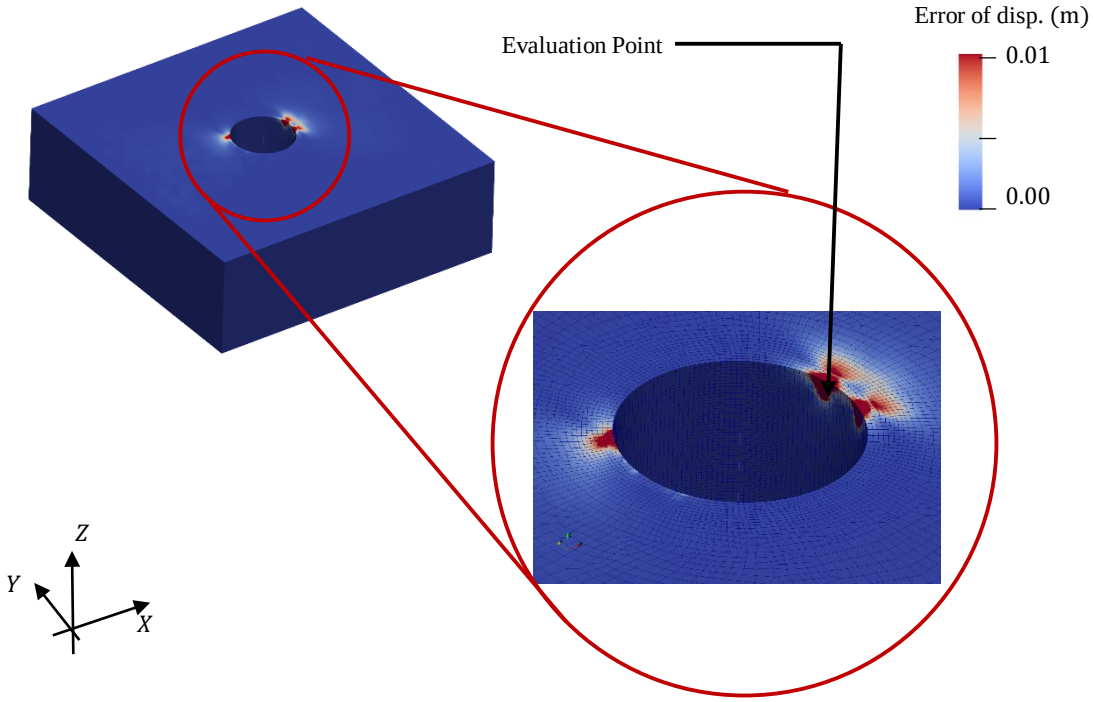

Figure 5.2: Difference of the displacement at 74.4 (s)

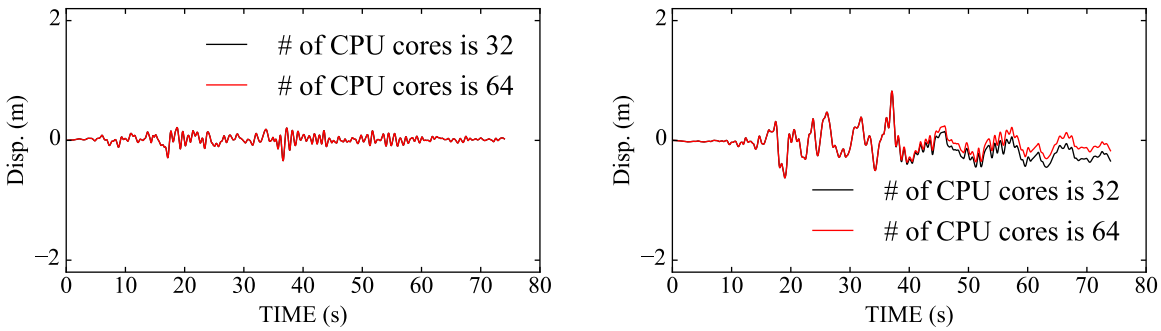

[1] x-direction [2] z-direction

Figure 5.3: Displacement of soil at the evaluation point

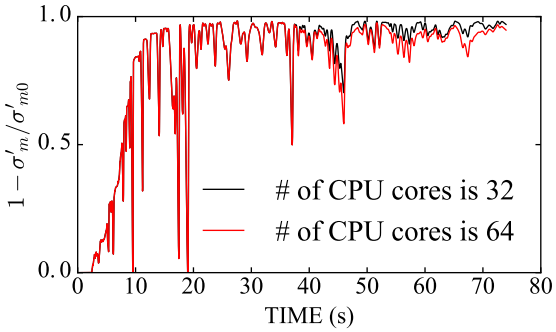

Figure 5.4: Time history of pore water pressure ratio, 1-σ'_m/σ'_{m0}, near the evaluation point (σ'_m: effective stress; σ'_{m0}: initial effective stress)

Table 5.1: Shear stiffness near the evaluation point

soil	beam element
4.2×10^3 (kN)	1.2×10^{10} (kN)

5.3 Quadruple precision in CG method

First of all, we use a convectional CG method for a quadruple precision instead of the adaptive CG method which is explained in Chapter 4. In CG method, parallel computation is used in matrix-vector product and inner dot. Parallel computation in matrix-vector doesn't change the order of calculation so that solution doesn't change. On the other hand, parallel computation in inner dot changes the order of calculation so that we use quadruple precision in inner dot of CG method.

Quadruple precision takes more computational time than double precision. We evaluate CPU time in quadruple precision with the FEM model which is shown in Section4.7.1. Table 5.2 shows the CPU time of inner dot in double and quadruple precision. Quadruple precision takes more than 20 times time than double precision. Table 5.3 shows the CPU time of solver in double and quadruple precision. Quadruple precision takes about one and a half times time than double precision. This is a demerit of quadruple precision

Table 5.2: CPU time of inner dot
(number of CPU cores is 64)

double precision	quadruple precision
2.84×10^{-3} (s)	6.82×10^{-2} (s)

Table 5.3: CPU time of the CG method
(number of CPU cores is 64)

double precision	quadruple precision
7.9 (s)	11.5 (s)

5.4 Quadruple precision in forming global matrix and vector

We use quadruple precision in forming global matrix and vector of the equation solved by CG method. But parallel performance of the forming global matrix in quadruple precision is a quite bad. The reason of this bad parallel performance is a critical section in a parallel computing, which prevents processors to access a share variable at the same time.

We introduce a multi-color ordering to remove the critical section. This ordering groups elements by color. Elements in the same group are not adjacent to each other (Fig.5.5). Parallel assembling local matrices in the same groups prevents processors to access a share variable at the same time without critical section. Table 5.4 and Fig. 5.6 show CPU time and parallel performance of forming global matrix of the FEM model which is shown in Section4.7.1. They shows a good parallel performance with 64 CPU cores.

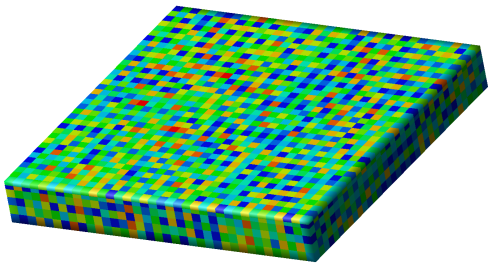

Figure 5.5: Multi-Color ordering

Table 5.4: CPU time of forming global matrix (NP is the number of processors)

number of CPU cores	quadruple precision	quadruple precision with multi-color method
1	196.3 (s)	196.3 (s)
16	19.6	16.2
32	20.2	9.0
64	25.0	5.3

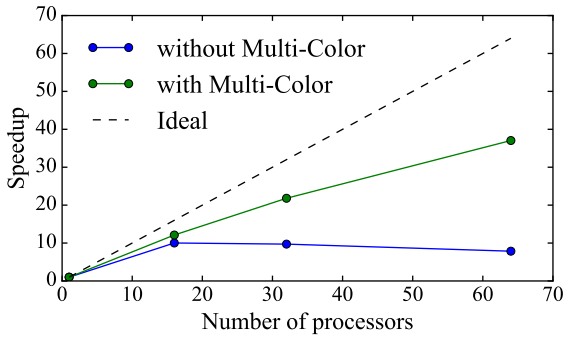

Figure 5.6: Strong scaling of forming global matrix in quadruple precision

5.5 Numerical Experiments

We did numerical tests of seismic response analysis with three FEM models in double and quadruple precision and check the ill behavior of the solution. We use the adaptive CG method which is explained in Chapter4 for the analysis in double precision.

There FEM models for the seismic response analysis are follows; 1) soil with horizontal layers; 2) soil with a pile foundation; 3) soil with a underground structure. FEM models of 2) and 3) are shown in Chapter 4.

5.5.1 Soil with horizontal layers (Case A)

Firstly we did a seismic response analysis with the FEM model of soil with the horizontal layers. Shapes and material properties are shown in Fig. 5.7 and Table 5.5. Only layer 3 of soil is a liquefaction layer. Input ground motion is shown in Fig. 4.2.

Fig. 5.8 shows the time history of difference and Fig. 5.9 shows the time history of dis-

placement of the node which has the max error. There is little difference of displacement with double precision.

Table 5.6 shows the max difference of displacement in double and quadruple precision. There is no difference in quadruple precision.

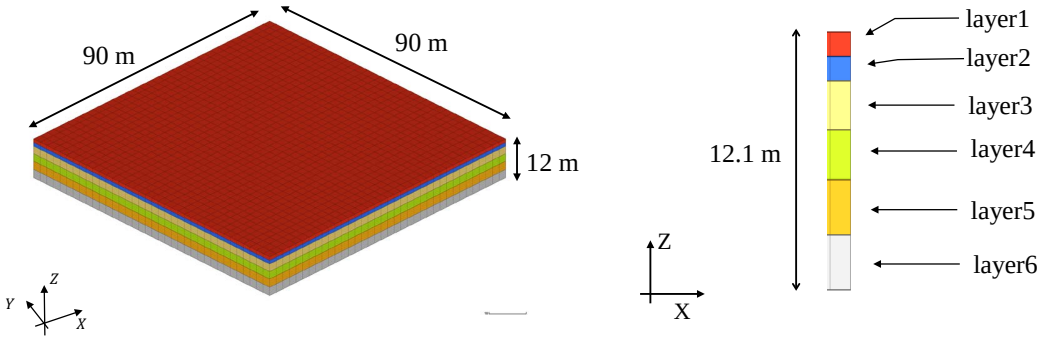

[1] soil [2] soil layer

Figure 5.7: FEM model of soil with pile foundation

Table 5.5: input parameter for soil

	ρ (t/m^3)	Vs (m/s)	G_{ma} (kPA)	ϕ_f (deg)	h_{max}	
layer 1	1.60	132	27950	39.0	0.24	-
layer 2	1.90	198	74800	42.0	0.24	-
layer 3	1.90	198	74800	42.0	0.24	liquefaction layer
layer 4	2.00	252	127100	43.9	0.24	-
layer 5	2.10	286	172030	43.9	0.24	-
layer 6	2.10	354	263530	43.9	0.24	-

ρ: density; Vs: shear wave velocity; G_{ma}: elastic shear modulus at a confining pressure; ϕ_f: shear resistance angle; h_{max}: damping

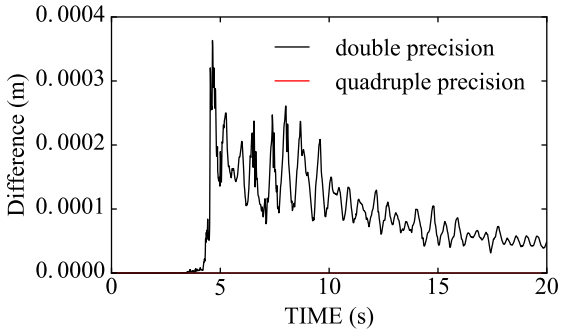

Figure 5.8: Time history of the difference of the displacement

Table 5.6: Max difference of displacement

double precision	quadruple precision
3.6×10^{-4} (m)	0.0 (m)

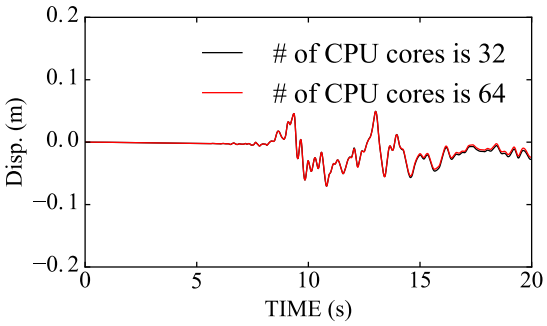

[1] x-direction

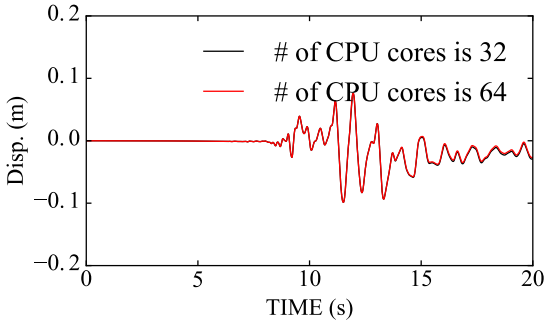

[2] y-direction

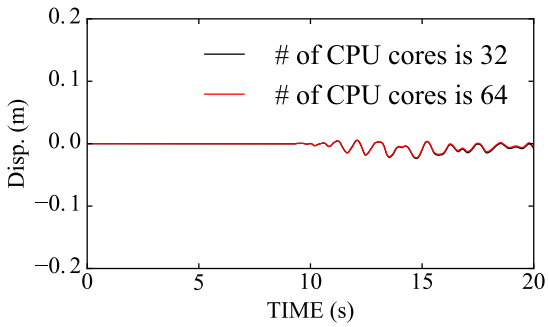

[3] z-direction

Figure 5.9: Displacement of soil with horizontal layers

5.5.2 Soil with a pile foundation (Case B)

Next, we did a numerical test with FEM model for soil with pile foundations which is shown in Chapter4

Fig. 5.10 shows the time history of the difference and Fig. 5.11 shows the displacement of the node which has the max error. There is little difference of the displacement. Shear stiffness of the beam element is 1000 times than that of the soil near the node which has the max error (See Table 5.8). Table 5.7 shows the max difference of displacement in double and quadruple precision. There is no difference of the displacement in quadruple precision.

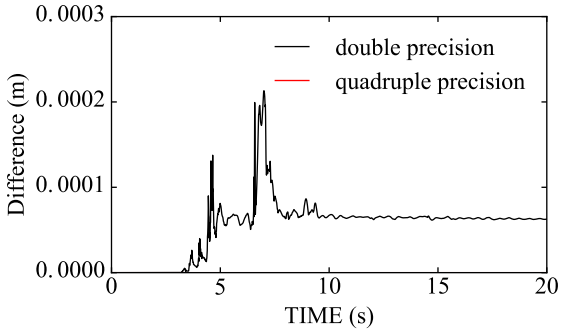

Figure 5.10: Time history of the difference of the displacement

Table 5.7: Max difference of displacement

double precision	quadruple precision
2.0×10^{-4} (m)	0.0 (m)

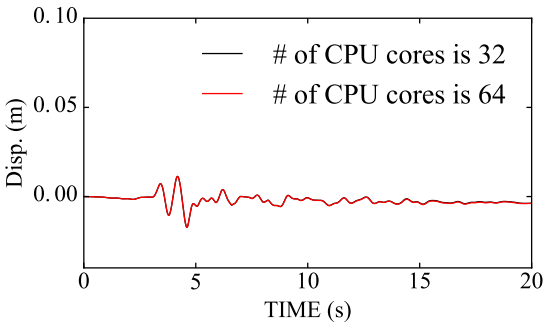

[1] x-direction

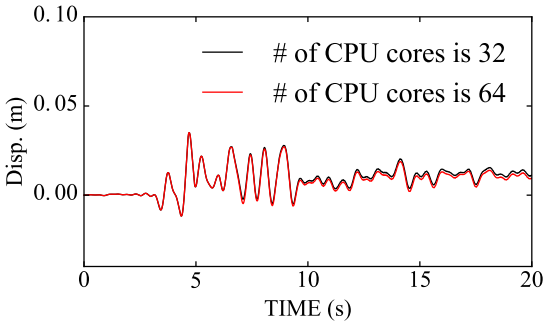

[2] y-direction

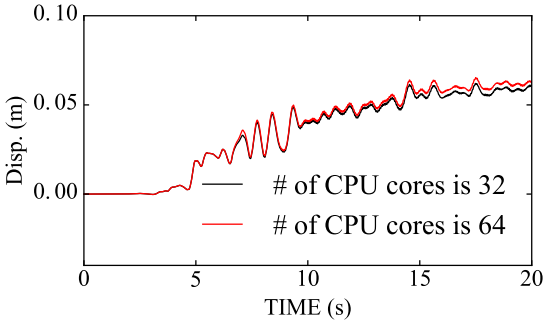

[3] z-direction

Figure 5.11: Displacement of soil with the pile foundation

Table 5.8: Shear stiffness

soil	beam element
8.9×10^{3} (kN)	1.0×10^{7} (kN)

5.5.3 Soil with underground structure (Case C)

Finally, we did a numerical test with FEM model for soil with an underground structure which is shown in Chapter 4

Fig. 5.12 shows the time history of the difference in double precision and quadruple precision. Table shows the max difference of displacement in double and quadruple precision. There is no difference of the displacement in quadruple precision.

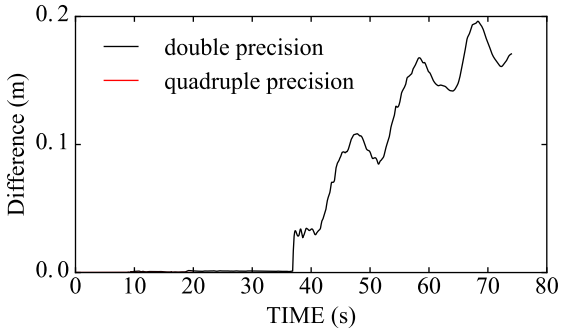

Figure 5.12: Time history of the difference of the displacement

Table 5.9: Max difference of displacement

double precision	quadruple precision
1.9×10^{-1} (m)	0.0 (m)

5.5.4 Discussions

We summarize and discuss the results of the numerical experiments. Table 5.10 shows the displacement errors of all numerical tests. There is a large difference with the the FEM model of soil with the underground structure. However, except this model, there is little difference in double precision computation so that we don't need a quadruple precision for every numerical analysis. There is no difference in quadruple precision in all cases. It mean that there is no difference in other solutions of FEM model, like strain, stress, velocity, etc.

Table 5.10 shows the shear stiffness of soil and structure and the condition of the interface between soil and structure. In the FEM model of soil with the underground structure, there

is a large difference of the shear stiffness. It might affect the ill behavior. A condition of the interface might affect the the ill behavior too. The difference of the solution occurred at the interface. But there is little difference of the displacement in x-direction which is constrained with a displacement of elastic beam elements. On the other hand, there is a large difference of the displacement in z-direction of the nodes is not constrained.

We should use the CG method in a quadruple precision as a verification tool considering a gap of shear stiffness between soil and structure and a condition of the interface

Table 5.10: Maximum displacement errors

	double precision	quadruple precision
Case A	3.6×10^{-4} (m)	0.0 (m)
Case B	2.0×10^{-4} (m)	0.0 (m)
Case C	1.9×10^{-1} (m)	0.0 (m)

Table 5.11: Condition of boundary between soil and structure

	shear stiffness liquefaction layer of soil	shear stiffness structure element	interface between soil and structure
Case A	7.2×10^{3} (kN)	-	-
Case B	8.9×10^{3} (kN)	1.0×10^{7} (kN)	rigid joint
Case C	4.2×10^{3} (kN)	1.2×10^{10} (kN)	slippage

5.6 Conclusion

In this chapter, we develop the HPC-FEM with a quadruple precision to fix the ill behavior. We did three seismic response analysis with the FEM model which consists in liquefaction layers of soil and structures and checked whether the HPC-FEM can fix the ill behavior. In all cases, the HPC-FEM fixed the the ill behavior

Chapter 6

PostProcess based on Meta-Modeling theory

6.1 Introduction

In design and evaluation works in the field of civil engineering, structure element, like beam and shell is mainly used for a FEM model [52]. But a structure element model simplifies shapes of a structure and takes much time and human resources to be constructed appropriately. On the other hand, solid element model can reflect shapes of a structure and can be made in an automated manner [12]. In a viewpoint of high fidelity and efficient construction, utilization of a solid element model is needed.

Although use of a solid element model is inevitable, but there is a problem in PostProcess to evaluate a FEM model with a large DOF. Civil engineers are used to design end evaluation works based on structure element components, like sectional force. In fact a structure element has advantage to deal with the average deformation and sectional force of a structure and help the engineers to grasp overall behaviors of a structure. This problem prevents frequent usage of solid element model. Therefore we need a conversion method from solid element solutions, like displacement and stress, to structure element solutions, like deformation and sectional force.

When a solid element solution is given, a typical conversion method sets a cross section

to evaluate and calculates displacement or stress on this section and then computes structure components by surface integration [48]. Such conversion is time consuming when a large-scale analysis is made. This method computes structure components only for a specified cross section and can't give a overview of the entire domain. In addition, this method lacks the physical background which guarantee the consistency between the solid and structure element solution.

According to the meta-modeling theory, we are able to convert a solid element model to a structure element model by satisfying the consistency with the original solid element model[22, 27, 47]. The meta-modeling theory constructs a structure model that is a consistent with a continuum model (or a solid element model) by solving the Lagrangian of continuum mechanics with a mathematical approximation. The previous studies develop the conversion method from solid element model to Bernoulli-Euler beam [26] in a Cartesian coordinate system. In this chapter, we seek to develop this conversion method to Timoshenko-beam, Mindlin–Reissner plate[34] and shell[8, 43] in a curved coordinate system which are most often used in practice.

The contents of this chapter are as follows. First we explain the meta-modeling theory and construct the governing equation of Timoshenko-beam and Mindlin–Reissner plate in Section 6.2. Then, in Section 6.3, we formulate the conversion method from solid element solution to structure element solution, curved beam and shell. With this method, did numerical tests with a cantilever, a plate and a cylinder to examine the capability of the proposed method.

6.2 Meta-Modeling Theory

In continuum mechanics, a boundary value problem respect to displacement function, $\mathbf{u}$, is solved for a quasi-static deformation problem. With an assumption of infinitesimally small deformation and linear isotropic elasticity, this boundary value problem is converted to a variational problem of using a Lagrangian, $\mathcal{L}$,

$$\begin{aligned} \mathcal{L}[\epsilon] &= \int_V \left(\frac{1}{2} \epsilon : \mathbf{c} : \epsilon \right) \mathrm{d}V \\ &= \int_V \left(\frac{1}{2} sym\{\nabla \mathbf{u}\} : \mathbf{c} : sym\{\nabla \mathbf{u}\} \right) \mathrm{d}V, \end{aligned} \tag{6.1}$$

where ϵ and $\mathbf{c}$ is strain tensor and elasticity tensor. ϵ is computed as $\epsilon = sym\{\nabla \mathbf{u}\}$ where sym stands for the symmetric part of the second-order tensor and ∇ is stands for spatial differentiation operator. And V is the domain of a target body. So the Lagrangian is also a function of displacement. Solving the variational problem, $\delta\mathcal{L} = \mathcal{L}[\mathbf{u} + \delta\mathbf{u}] - \mathcal{L}[\mathbf{u}] = 0$, we get the following governing equation,

$$\nabla \cdot (\mathbf{c} : sym\{\nabla \mathbf{u}\}) = \nabla \cdot \sigma = 0, \quad (\because \ \sigma = \ \mathbf{c} : \epsilon) \tag{6.2}$$

σ is stress tensor.

In the meta-modeling theory[22], we use the variational problem of $\mathcal{L}^*[\mathbf{u}, \sigma]$,

$$\begin{aligned} \mathcal{L}^*[\mathbf{u}, \sigma] &= \int_V \left(\sigma : \epsilon - \frac{1}{2} \sigma : \mathbf{c}^{-1} : \sigma \right) \mathrm{d}V \ \ \left(\epsilon = \ \mathbf{c}^{-1} : \sigma \right) \\ &= \int_V \left(\sigma : sym\{\nabla \mathbf{u}\} - \frac{1}{2} \sigma : \mathbf{c}^{-1} : \sigma \right) \mathrm{d}V \end{aligned} \tag{6.3}$$

We can derive the stress-strain relation and the governing equation of continuum mechanics. The variational problem of $\mathcal{L}^*$ respect to σ, $\mathcal{L}^*[\sigma + \delta\sigma] - \mathcal{L}^*[\sigma] = 0$, yields stress-strain relation,

$$\sigma = \ \mathbf{c} : \epsilon. \tag{6.4}$$

The variational problem of $\mathcal{L}^*$ respect to $\mathbf{u}$, $\mathcal{L}^*[\mathbf{u}+\delta\mathbf{u}]-\mathcal{L}^*[\mathbf{u}] = 0$, yields the governing equation of Eq.(6.2).

In the same way, we can derive the stress-strain relation and the governing equation of structure model with the approximation of displacement and stress. For example, we set the approximation of displacement and stress for truss theory as follows:

$$\mathbf{u}(\mathbf{x}) = \{u_1, \ u_2, \ u_3\} \approxeq \{u_1(x_1), \ 0, \ 0\}^T \tag{6.5}$$

$$\sigma(\mathbf{x}) = \begin{pmatrix} \sigma_{11} & \sigma_{12} & \sigma_{13} \\ & \sigma_{22} & \sigma_{23} \\ sym. & & \sigma_{33} \end{pmatrix} \approxeq \begin{pmatrix} \sigma_{11} & 0 & 0 \\ & 0 & 0 \\ sym. & & 0 \end{pmatrix} \tag{6.6}$$

where **x** stands for a three-dimensional coordinate. With these approximation, $\delta\mathcal{L}^* = 0$ respect to σ yields $\sigma_{11} = E\epsilon_{11}$, and then $\delta\mathcal{L}^* = 0$ respect to u_1 yields

$$AE\frac{\partial^2 u_1}{\partial x_1^2} = 0, \tag{6.7}$$

where A is the area of cross section of the truss and E is Young's modules.

Based on meta-modeling theory, Structure model can be constructed by solving the Lagrangian of continuum mechanics with a mathematical approximation.

6.2.1 Timoshenko-Beam

We derive the stress-strain relation and the governing equation of Timoshenko-Beam based on meta-modeling method. We use the following approximation of displacement and stress:

$$\mathbf{u} \approx \{-x_3\theta(x_1), 0, u_3(x_1)\}^T \tag{6.8}$$

$$\sigma \approx \begin{pmatrix} \sigma_{11} & 0 & \sigma_{13} \\ & 0 & 0 \\ sym. & & 0 \end{pmatrix}, \tag{6.9}$$

where θ is a rotation around x_2 axis (See Fig.6.1).

With this approximation, $\delta\mathcal{L}^* = 0$ respect to σ derives the following stress-strain relation:

$$\mathcal{L}^*[\sigma + \delta\sigma, \epsilon] - \mathcal{L}^*[\sigma, \epsilon] = \int_V \left\{ \left(\epsilon_{11} - \frac{\sigma_{11}}{E}\right)\delta\sigma_{11} + \left(\epsilon_{13} - \frac{\sigma_{13}}{2G}\right)\delta\sigma_{13} \right\} \mathrm{d}v = 0, \tag{6.10}$$

$$\therefore \begin{array}{l} \sigma_{11} = E\epsilon_{11} \\ \sigma_{13} = 2G\epsilon_{13}, \end{array} \tag{6.11}$$

where E is Young's modules and G is shear modules. There equations are law of Hooke, which is used in a beam model. In Timosheko-Beam model, G is replace with $G' = kG$. k is a shear correction factor.

With this stress-strain relation of Eq.(6.11), $\delta\mathcal{L}^* = 0$ respect to **u** with a distributed load

$q(x_1)$ yields

$$\begin{aligned}
&\int \{EI\theta'\delta\theta' + kAG(u_3' - \theta)(\delta u_3' - \delta\theta)\}\mathrm{d}x_1 - \int q\delta u_3 \mathrm{d}x_1 \\
&= -\int \{EI\theta'' + kAG(u_3' - \theta)\}\delta\theta \mathrm{d}x_1 - \int \{kAG(u_3'' - \theta') + q\}\delta u_3 \mathrm{d}x_1 \\
&=0,
\end{aligned} \tag{6.12}$$

$$\begin{aligned}
&EI\theta'' + kAG(u_3' - \theta) = 0 \\
\therefore \quad & \\
&q + kAG(u_3'' - \theta') = 0,
\end{aligned} \tag{6.13}$$

where

$$A = \int \mathrm{d}x_2 \mathrm{d}x_3$$

$$I = \int (x_3)^2 \mathrm{d}x_2 \mathrm{d}x_3$$

and prime stands for derivative with respect to x_1.

Rearranging these equation respect to u_3, we can derive the following governing equation of Timoshenko beam [41].

$$EIu_3'''' = q - \frac{EI}{kGA}q'' \tag{6.14}$$

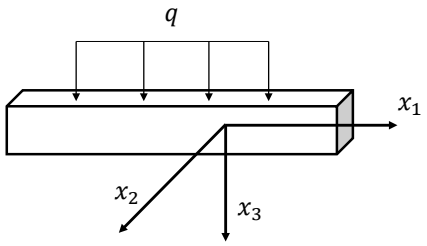

Figure 6.1: Schematic view of beam with a distributed load q and coordinate system

6.2.2 Mindlin Plate

We derive the stress-strain relation and the governing equation of Mindlin-Plate based on meta-modeling method. We use the following approximation of displacement and stress:

$$u \approx \{-x_3\theta_2(x_1, x_2), -x_3\theta_1(x_1, x_2), u_3(x_1, x_2)\}^T \tag{6.15}$$

$$\sigma \approx \begin{pmatrix} \sigma_{11} & \sigma_{12} & \sigma_{13} \\ & \sigma_{22} & \sigma_{23} \\ sym. & & 0 \end{pmatrix}, \tag{6.16}$$

$$\tag{6.17}$$

where θ_i is a rotation around x_i axis (See Fig.6.2).

With this approximation, $\delta\mathcal{L}^* = 0$ respect to σ derives the following stress-strain relation:

$$\begin{Bmatrix} \epsilon_{11} \\ \epsilon_{22} \\ 2\epsilon_{12} \\ 2\epsilon_{23} \\ 2\epsilon_{31} \end{Bmatrix} = \begin{pmatrix} 1/E & -\nu/E & & & \\ -\nu/E & 1/E & & & \\ & & 1/G & & \\ & & & 1/G & \\ & & & & 1/G \end{pmatrix} \begin{Bmatrix} \sigma_{11} \\ \sigma_{22} \\ \sigma_{12} \\ \sigma_{23} \\ \sigma_{31} \end{Bmatrix} \tag{6.18}$$

where ν is Poisson's ratio. In Midline-Plate model, shear stress out of plane is adjusted with a shear correction factor,

$$\begin{aligned} \sigma_{23} &= 2kG\epsilon_{23} \\ \sigma_{31} &= 2kG\epsilon_{31} \end{aligned} \tag{6.19}$$

With this stress-strain relation, $\delta\mathcal{L}^* = 0$ respect to $\{u_3,\ \theta_1,\ \theta_2\}$ with a distributed load $q(x_1, x_2)$ yields the following governing equation of Midline-Plate model [36].

$$kGH\left(\nabla^2 u_3 + \Phi\right) = -q \tag{6.20}$$

$$D\frac{1-\nu}{2}\nabla^2\theta_2 + D\frac{1+\nu}{2}\frac{\partial\Phi}{\partial x_1} - kGH\left(\theta_2 + \frac{\partial u_3}{\partial x_1}\right) = 0 \tag{6.21}$$

$$D\frac{1-\nu}{2}\nabla^2\theta_1 + D\frac{1+\nu}{2}\frac{\partial\Phi}{\partial x_2} - kGH\left(\theta_1 + \frac{\partial u_3}{\partial x_2}\right) = 0 \tag{6.22}$$

where

$$D = \frac{EH^3}{12\,(1-\nu^2)},\ \nabla = \frac{\partial^2}{\partial^2 x_1} + \frac{\partial^2}{\partial^2 x_2},\ \Phi = \frac{\partial\theta_1}{\partial x_2} + \frac{\partial\theta_2}{\partial x_1} \tag{6.23}$$

and H is a thickness of plate.

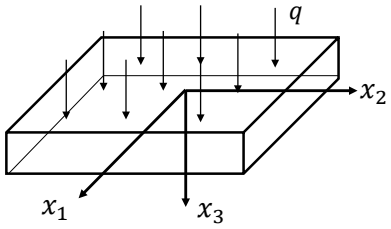

Figure 6.2: Schematic view of plate with a distributed load q and coordinate system

6.3 Conversion of solid element solution to structure element solution

Based on the meta-modeling theory, a structure element solution is regarded as an approximate numerical solution of a continuum mechanics solution (or a solid element solution). It is natural to make the conversion from a solid element solution to a structure element solution.

In order to relate a solution of a solid element, $\mathbf{u}_\mathrm{s}$, to a solution of a structure element, $\mathbf{u}_\mathrm{c}$, we introduce the following the error function:

$$\mathcal{E} = \int |\mathbf{u}_\mathrm{s} - \mathbf{u}_\mathrm{c}|^2 \,\mathrm{d}V, \tag{6.24}$$

where $||^2$ is the square of vector, for example, $|\mathbf{u}|^2 = u_i u_i$. When a solid element solution is given, we can find a structure element solution which minimizes $\mathcal{E}$. In finite element method,

$\mathbf{u}_c$ and $\mathbf{u}_s$ are discredited in space and computed in terms of the nodal displacement.

In this section, we formulate the conversion of a solution of a solid element model to a solution of the curved beam model model and shell element model.

6.3.1 Curved beam

We formulate the conversion of solution of a solid element model to solution of the curved beam model model.

position vector

We define a position vector, $\overline{\mathbf{X}}$, which moves on the center of the cross section of a curved beam and orthonormal vectors $\{\mathbf{E}_1,\ \mathbf{E}_2,\ \mathbf{E}_3\}$ at the center of the cross section (See Fig. 6.3). We can write a position vector, $\mathbf{x}_s$ in a curved beam as follows:

$$\mathbf{x}_s = \overline{\mathbf{X}} + \eta\mathbf{E}_2 + \ \zeta\mathbf{E}_3 \tag{6.25}$$

displacement vector

With an assumption of infinitesimally small deformation, we can write displacement of a curved beam, $\mathbf{u}_s$, as follows:

$$\mathbf{u}_s = \overline{\mathbf{U}} + \eta\mathbf{\Theta} \times \mathbf{E}_2 + \ \zeta\mathbf{\Theta} \times \mathbf{E}_3\ , \tag{6.26}$$

where

$\overline{\mathbf{U}}$: Displacement at the center of the cross section

$\mathbf{\Theta}$: Infinitesimal rotation vector at the center of the cross section

and "$\times$" stands for cross product.

Approximation with shape functions

We divide the line which penetrate through the center of the cross section by 1D elements and approximate position and displacement by nodal values and shape functions as follows:

$$\mathbf{x}_\mathrm{s} \simeq \mathbf{x}_\mathrm{s}(\xi,\eta,\zeta) = \sum N^{(\alpha)}(\xi)\left(\overline{\mathbf{X}}^{(\alpha)} + \eta\mathbf{E}_2^{(\alpha)} + \zeta\mathbf{E}_3^{(\alpha)}\right) \tag{6.27}$$

$$\begin{aligned}\mathbf{u}_\mathrm{s} \simeq \mathbf{u}_\mathrm{s}(\xi,\eta,\zeta) &= \sum N^{(\alpha)}(\xi)\left(\overline{\mathbf{U}}^{(\alpha)} + \eta\boldsymbol{\Theta}^{(\alpha)}\times\mathbf{E}_2^{(\alpha)} + \zeta\boldsymbol{\Theta}^{(\alpha)}\times\mathbf{E}_3^{(\alpha)}\right)\\ &= \sum N^{(\alpha)}(\xi)\left\{\overline{U}_i^{(\alpha)}\mathbf{E}_i^{(\alpha)} + \eta\left(\Theta_i^{(\alpha)}\mathbf{E}_i^{(\alpha)}\right)\times\mathbf{E}_2^{(\alpha)} + \zeta\left(\Theta_i^{(\alpha)}\mathbf{E}_i^{(\alpha)}\right)\times\mathbf{E}_3^{(\alpha)}\right\}\\ &= \sum N^{(\alpha)}(\xi)\left(\overline{U}_i^{(\alpha)}\mathbf{E}_i^{(\alpha)} - \eta\Theta_3^{(\alpha)}\mathbf{E}_1^{(\alpha)} + \zeta\Theta_2^{(\alpha)}\mathbf{E}_1^{(\alpha)}\right)\end{aligned} \tag{6.28}$$

where

$$\begin{aligned} N^{(\alpha)}(\xi) &: \ \alpha\text{th shape function of 1D element}\\ \overline{\mathbf{X}}^{(\alpha)} &: \ \alpha\text{th nodal position vector}\\ \overline{\mathbf{U}}^{(\alpha)} &: \ \alpha\text{th nodal displacement vector}\\ \boldsymbol{\Theta}^{(\alpha)} &: \ \alpha\text{th nodal infinitesimal rotation vector}\\ \mathbf{E}^{(\alpha)} &: \ \text{Unit orthogonal vector at the } \alpha\text{th node}\end{aligned}$$

In this Eq.(4), we assume that the beam is not twisted so that $\Theta_1^{(\alpha)} = 0$ for simplicity.

Derivation of a linear equation by minimization of $\mathcal{E}$

Substituting Eq.(6.24) into the error function of Eq. (6.24),

$$\begin{aligned}\mathcal{E} &= \int |\mathbf{u}_\mathrm{c} - \mathbf{u}_\mathrm{s}|^2 \,\mathrm{d}V\\ &= \int |\mathbf{u}_\mathrm{c} - \sum N^{(\alpha)}(\xi)\left(\overline{U}_i^{(\alpha)}\mathbf{E}_i^{(\alpha)} - \eta\Theta_3^{(\alpha)}\mathbf{E}_1^{(\alpha)} + \zeta\Theta_2^{(\alpha)}\mathbf{E}_1^{(\alpha)}\right)|^2 \,\mathrm{d}V,\end{aligned} \tag{6.29}$$

we compute the partial derivative of $\mathcal{E}$ with respect to $\overline{U}_i^{(\alpha)}$ and $\Theta_i^{(\alpha)}$ which are unknown values,

$$\frac{\partial\mathcal{E}}{\partial U_i^{(\alpha)}} = \int 2N^{(\alpha)}\mathbf{E}_i^{(\alpha)}\cdot\{\mathbf{u}_\mathrm{c} - \mathbf{u}_\mathrm{s}(\xi,\eta,\zeta)\}\,\mathrm{d}V = 0 \ \ (i=1,2,3) \tag{6.30}$$

$$\frac{\partial \mathcal{E}}{\partial \Theta_2^{(\alpha)}} = \int \zeta N^{(\alpha)} \mathbf{E}_1^{(\alpha)} \cdot \{\mathbf{u}_c - \mathbf{u}_s(\xi, \eta, \zeta)\} \, dV = 0 \tag{6.31}$$

$$\frac{\partial \mathcal{E}}{\partial \Theta_3^{(\alpha)}} = -\int \eta N^{(\alpha)} \mathbf{E}_1^{(\alpha)} \cdot \{\mathbf{u}_c - \mathbf{u}_s(\xi, \eta, \zeta)\} \, dV = 0, \tag{6.32}$$

where dot stands for inner product.

Rearranging Eq.(6.30), (6.31) and (6.32) according to the unknown values, we obtain the following equations

$$\int \{N^{(\alpha)} \mathbf{E}_i^{(\alpha)} \cdot \mathbf{u}_c - N^{(\alpha)} N^{(\beta)} \left(g_{ij}^{(\alpha\beta)} U_j^{(\beta)} + g_{i1}^{(\alpha\beta)} \left(-\eta \Theta_3^{(\beta)} + \zeta \Theta_2^{(\beta)} \right) \right\} dV = 0 \tag{6.33}$$

$$(i = 1, 2, 3)$$

$$\int \{\zeta N^{(\alpha)} \mathbf{E}_2^{(\alpha)} \cdot \mathbf{u}_c - N^{(\alpha)} N^{(\beta)} \left(\zeta g_{1j}^{(\alpha\beta)} U_j^{(\beta)} + g_{11}^{(\alpha\beta)} \left(-\eta\zeta \Theta_3^{(\beta)} + \zeta^2 \Theta_2^{(\beta)} \right) \right\} dV = 0 \tag{6.34}$$

$$\int \{-\eta N^{(\alpha)} \mathbf{E}_1^{(\alpha)} \cdot \mathbf{u}_c - N^{(\alpha)} N^{(\beta)} \left(-\eta g_{1j}^{(\alpha\beta)} U_j^{(\beta)} + g_{11}^{(\alpha\beta)} \left(\eta^2 \Theta_3^{(\beta)} - \eta\zeta \Theta_2^{(\beta)} \right) \right\} dV = 0, \tag{6.35}$$

where

$$g_{ij}^{(\alpha\beta)} = \mathbf{E}_i^{(\alpha)} \cdot \mathbf{E}_j^{(\beta)} \quad (i, j = 1, 2, 3) \tag{6.36}$$

Assembling these equations of all nodes, we get the following linear equation, $\mathbf{A}\mathbf{x} = \mathbf{b}$,

$$\begin{pmatrix} \mathbf{A}^{(11)} & \mathbf{A}^{(12)} & \cdots & \mathbf{A}^{(1n)} \\ & \mathbf{A}^{(22)} & & \\ & & \ddots & \\ & & & \mathbf{A}^{(nn)} \end{pmatrix} \begin{pmatrix} \mathbf{X}^{(1)} \\ \mathbf{X}^{(2)} \\ \vdots \\ \mathbf{X}^{(n)} \end{pmatrix} = \begin{pmatrix} \mathbf{b}^{(1)} \\ \mathbf{b}^{(2)} \\ \vdots \\ \mathbf{b}^{(n)} \end{pmatrix}, \ (n \text{ is the numer of nodes}) \tag{6.37}$$

where

$$\mathbf{X}^{(\alpha)} = \left\{ U_{\mathbf{1}}^{(\alpha)}, U_{\mathbf{2}}^{(\alpha)}, U_{\mathbf{3}}^{(\alpha)}, \Theta_2^{(\alpha)}, \Theta_3^{(\alpha)} \right\}^T$$

$$\mathbf{b}^{(\alpha)} = \int N^{(\alpha)} \left\{ b_{\mathbf{1}}^{(\alpha)}, b_2^{(\alpha)}, b_{\mathbf{3}}^{(\alpha)}, b_4^{(\alpha)}, b_5^{(\alpha)} \right\}^T dV$$

$$\mathbf{A}^{(\alpha\beta)=}\int N^{(\alpha)}N^{(\beta)}\begin{pmatrix} A_{11}^{(\alpha\beta)} & A_{12}^{(\alpha\beta)} & \cdots & A_{15}^{(\alpha\beta)} \\ & A_{22}^{(\alpha\beta)} & & \\ & & \ddots & \\ Sym. & & & A_{55}^{(\alpha\beta)} \end{pmatrix}\mathrm{d}V,$$

and

$$\begin{aligned} A_{ij}^{(\alpha\beta)} &= g_{ij}^{(\alpha\beta)} \ (i,j=1,2,3) \\ A_{44}^{(\alpha\beta)} &= \zeta^2 g_{11}^{(\alpha\beta)} \\ A_{55}^{(\alpha\beta)} &= \zeta^2 g_{11}^{(\alpha\beta)} \\ A_{45}^{(\alpha\beta)} &= -\eta\zeta g_{11}^{(\alpha\beta)} \\ A_{i4}^{(\alpha\beta)} &= -\zeta g_{i1}^{(\alpha\beta)} \ (i=1,2,3) \\ A_{i5}^{(\alpha\beta)} &= \ \eta g_{i1}^{(\alpha\beta)} \ (i=1,2,3) \end{aligned}$$

$$\begin{aligned} b_{\mathbf{i}}^{(\alpha)} &= \mathbf{E}_i^{(\alpha)} \cdot \mathbf{u}_{\mathrm{c}} \\ b_{\mathbf{4}}^{(\alpha)} &= \zeta \mathbf{E}_1^{(\alpha)} \cdot \mathbf{u}_{\mathrm{c}} \\ b_{\mathbf{5}}^{(\alpha)} &= -\eta \mathbf{E}_1^{(\alpha)} \cdot \mathbf{u}_{\mathrm{c}} \end{aligned}$$

$$\int f\mathrm{d}V = \int f(x_1,x_2.x_3)\mathrm{d}x_1\mathrm{d}x_2\mathrm{d}x_3 = \int f(\xi,\eta,\zeta)\left|\frac{\partial(x_1,x_2,x_3)}{\partial(\xi,\eta,\zeta)}\right|\mathrm{d}\xi\mathrm{d}\eta\mathrm{d}\zeta.$$

We can get the solution of the curved beam which minimizes $\mathcal{E}$ by solving the Eq.(6.37).

Straight beam

When a beam is straight and the potion vector, $\overline{\mathbf{X}}$, moves on a straight line, we just use the following equations instead of Eq.(6.36),

$$g_{ij}^{(\alpha\beta)} = \begin{cases} 1 & (i=j) \\ 0 & (i\neq j) \end{cases} \left(\because \mathbf{E}_i^{(\alpha)} = \mathbf{E}_i^{(\beta)}\right) \tag{6.38}$$

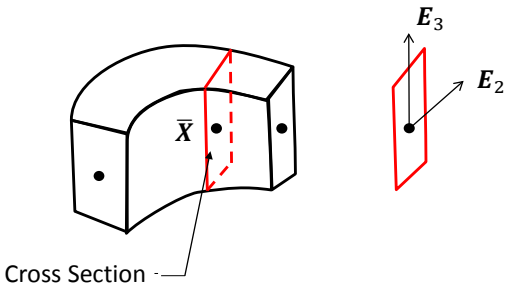

Figure 6.3: Coordinate system and position vector of curved beam

6.3.2 Shell

We formulate the conversion method of solution of a solid element model to solution of the shell model in the same procedures as the curved beam section.

position vector

We define a position vector, $\overline{\mathbf{X}}$, which moves on the midsurface of a shell and orthonormal vectors $\{\mathbf{E}_1,\ \mathbf{E}_2,\ \mathbf{E}_3\}$ on the midsurface (See Fig.6.4). We can write a position vector, $\mathbf{x}_s$ in a shell as follows:

$$\mathbf{x}_s = \overline{\mathbf{X}} + \zeta \mathbf{E}_3 \tag{6.39}$$

displacement vector

With an assumption of infinitesimally small deformation, we can write displacement of a shell, $\mathbf{u}_s$, as follows:

$$\mathbf{u}_s = \overline{\mathbf{U}} + \zeta\ \boldsymbol{\Theta} \times \mathbf{E}_3 \tag{6.40}$$

where

$\overline{\mathbf{U}}$: Displacement at the midsurface

$\boldsymbol{\Theta}$: Infinitesimal rotation vector at the midsurface

Approximation with shape functions

We divide the midsurface by 2D elements and approximate position and displacement by nodal values and shape functions as follows (See Fig. 6.5) ,

$$\mathbf{x}_{\mathrm{s}} \simeq \mathbf{x}_{\mathrm{s}}(\xi, \eta, \zeta) = \sum N^{(\alpha)}(\xi, \eta) \left(\overline{\mathbf{X}}^{(\alpha)} + \zeta \, \mathbf{E}_3^{(\alpha)} \right) \tag{6.41}$$

$$\begin{aligned} \mathbf{u}_{\mathrm{s}} \simeq \mathbf{u}_{\mathrm{s}}(\xi, \eta, \zeta) &= \sum N^{(\alpha)}(\xi, \eta) \left(\overline{\mathbf{U}}^{(\alpha)} + \zeta \boldsymbol{\Theta}^{(\alpha)} \times \mathbf{E}_3^{(\alpha)} \right) \\ &= \sum N^{(\alpha)}(\xi, \eta) \left\{ \overline{U}_i^{(\alpha)} \mathbf{E}_i^{(\alpha\ )} + \zeta \left(\Theta_i^{(\alpha)} \mathbf{E}_i^{(\alpha)} \right) \times \mathbf{E}_3^{(\alpha)} \right\} \\ &= \sum N^{(\alpha)}(\xi, \eta) \left(\overline{U}_i^{(\alpha)} \mathbf{E}_i^{(\alpha)} + \zeta \Theta_2^{(\alpha)} \mathbf{E}_1^{(\alpha)} - \zeta \Theta_1^{(\alpha)} \mathbf{E}_2^{(\alpha)} \right) \end{aligned} \tag{6.42}$$

where

$$\begin{aligned} N^{(\alpha)}(\xi, \eta) &: \ \alpha\text{th shape function of 2D element} \\ \overline{\mathbf{X}}^{(\alpha)} &: \ \alpha\text{th nodal position vector} \\ \overline{\mathbf{U}}^{(\alpha)} &: \ \alpha\text{th nodal displacement vector} \\ \boldsymbol{\Theta}^{(\alpha)} &: \ \alpha\text{th nodal infinitesimal rotation vector} \\ \mathbf{E}^{(\alpha)} &: \ \text{Unit orthogonal vector at the } \alpha\text{th node} \end{aligned}$$

In this Eq.(6.42), we assume $\Theta_3^{(\alpha)} = 0$ for simplicity.

Derivation of a linear equation by minimization of $\mathcal{E}$

Substituting Eq.(6.42) into the distance function of Eq.(6.24),

$$\begin{aligned} \mathcal{E} &= \int |\mathbf{u}_{\mathrm{c}} - \mathbf{u}_{\mathrm{s}}|^2 \, \mathrm{d}V \\ &= \int |\mathbf{u}_{\mathrm{c}} - \sum N^{(\alpha)}(\xi, \eta) \left(\overline{U}_i^{(\alpha)} \mathbf{E}_i^{(\alpha)} + \zeta \Theta_2^{(\alpha)} \mathbf{E}_1^{(\alpha)} - \zeta \Theta_1^{(\alpha)} \mathbf{E}_2^{(\alpha)} \right) |^2 \, \mathrm{d}V, \end{aligned} \tag{6.43}$$

we compute the partial derivative of $\mathcal{E}$ with respect to $\overline{U}_i^{(\alpha)}$ and $\Theta_i^{(\alpha)}$ which are unknown values,

$$\frac{\partial \mathcal{E}}{\partial U_i^{(\alpha)}} = \int 2N^{(\alpha)}\mathbf{E}_i^{(\alpha)} \cdot \{\mathbf{u}_c - \mathbf{u}_s(\xi,\eta,\zeta)\} \mathrm{d}V = 0 \ \ (i = 1,2,3) \tag{6.44}$$

$$\frac{\partial \mathcal{E}}{\partial \Theta_1^{(\alpha)}} = \int -\zeta N^{(\alpha)}\mathbf{E}_2^{(\alpha)} \cdot \{\mathbf{u}_c - \mathbf{u}_s(\xi,\eta,\zeta)\} \mathrm{d}V = 0 \tag{6.45}$$

$$\frac{\partial \mathcal{E}}{\partial \Theta_2^{(\alpha)}} = \int \zeta N^{(\alpha)}\mathbf{E}_1^{(\alpha)} \cdot \{\mathbf{u}_c - \mathbf{u}_s(\xi,\eta,\zeta)\} \mathrm{d}V = 0 \,. \tag{6.46}$$

Rearranging Eq.(6.44), (6.45) and (6.46) according to the unknown values, we obtain the following equations

$$\int \left\{ N^{(\alpha)}\mathbf{E}_i^{(\alpha)} \cdot \mathbf{u}_c - N^{(\alpha)}N^{(\beta)} \left(g_{ij}^{(\alpha\beta)} U_j^{(\beta)} - \ \zeta g_{i2}^{(\alpha\beta)} \Theta_1^{(\beta)} + \zeta g_{i1}^{(\alpha\beta)} \Theta_2^{(\beta)} \right) \right\} \mathrm{d}V = 0 \tag{6.47}$$

$$(i = 1,2,3) \tag{6.48}$$

$$\int \left\{ -\zeta N^{(\alpha)}\mathbf{E}_2^{(\alpha)} \cdot \mathbf{u}_c - N^{(\alpha)}N^{(\beta)} \left(-\zeta g_{2j}^{(\alpha\beta)} U_j^{(\beta)} + \zeta^2 g_{22}^{(\alpha\beta)} \Theta_1^{(\beta)} - \zeta^2 g_{21}^{(\alpha\beta)} \Theta_2^{(\beta)} \right) \right\} \mathrm{d}V = 0 \tag{6.49}$$

$$\int \left\{ \zeta N^{(\alpha)}\mathbf{E}_1^{(\alpha)} \cdot \mathbf{u}_c - N^{(\alpha)}N^{(\beta)} \left(\zeta g_{1j}^{(\alpha\beta)} U_j^{(\beta)} - \zeta^2 g_{12}^{(\alpha\beta)} \Theta_1^{(\beta)} + \zeta^2 g_{11}^{(\alpha\beta)} \Theta_2^{(\beta)} \right) \right\} \mathrm{d}V = 0 \tag{6.50}$$

where

$$g_{ij}^{(\alpha\beta)} = \mathbf{E}_i^{(\alpha)} \cdot \mathbf{E}_j^{(\beta)} \ \ (i,j = 1,2,3). \tag{6.51}$$

Assembling these equations of all nodes, we get the following linear equation, $\mathbf{Ax} = \mathbf{b}$,

$$\begin{pmatrix} \mathbf{A}^{(11)} & \mathbf{A}^{(12)} & \cdots & \mathbf{A}^{(1n)} \\ & \mathbf{A}^{(22)} & & \\ & & \ddots & \\ & & & \mathbf{A}^{(nn)} \end{pmatrix} \begin{Bmatrix} \mathbf{X}^{(1)} \\ \mathbf{X}^{(2)} \\ \vdots \\ \mathbf{X}^{(n)} \end{Bmatrix} = \begin{Bmatrix} \mathbf{b}^{(1)} \\ \mathbf{b}^{(2)} \\ \vdots \\ \mathbf{b}^{(n)} \end{Bmatrix}, \ (n \text{ is the number of nodes}) \tag{6.52}$$

where

$$\mathbf{X}^{(\alpha)} = \left\{ U_{\mathbf{1}}^{(\alpha)}, U_{\mathbf{2}}^{(\alpha)}, U_{\mathbf{3}}^{(\alpha)}, \Theta_1^{(\alpha)}, \Theta_2^{(\alpha)} \right\}^T$$

$$\mathbf{b}^{(\alpha)} = \int N^{(\alpha)} \left\{ b_{\mathbf{1}}^{(\alpha)}, b_2^{(\alpha)}, b_{\mathbf{3}}^{(\alpha)}, b_4^{(\alpha)}, b_5^{(\alpha)} \right\}^T \mathrm{d}V$$

$$\mathbf{A}^{(\alpha\beta)=}\int N^{(\alpha)}N^{(\beta)}\begin{pmatrix} A_{11}^{(\alpha\beta)} & A_{12}^{(\alpha\beta)} & \cdots & A_{15}^{(\alpha\beta)} \\ & A_{22}^{(\alpha\beta)} & & \\ & & \ddots & \\ Sym. & & & A_{55}^{(\alpha\beta)} \end{pmatrix}\mathrm{d}V$$

and the components are written as follows:

$$\begin{aligned} A_{ij}^{(\alpha\beta)} &= g_{ij}^{(\alpha\beta)} \ (i,j=1,2,3) \\ A_{44}^{(\alpha\beta)} &= \zeta^2 g_{22}^{(\alpha\beta)} \\ A_{55}^{(\alpha\beta)} &= \zeta^2 g_{11}^{(\alpha\beta)} \\ A_{45}^{(\alpha\beta)} &= -\zeta^2 g_{21}^{(\alpha\beta)} \\ A_{i4}^{(\alpha\beta)} &= -\zeta g_{i2}^{(\alpha\beta)} \ (i=1,2,3) \\ A_{i5}^{(\alpha\beta)} &= \ \zeta g_{i1}^{(\alpha\beta)} \ (i=1,2,3) \end{aligned}$$

$$\begin{aligned} b_{\mathbf{i}}^{(\alpha)} &= \mathbf{E}_i^{(\alpha)} \cdot \mathbf{u}_{\mathrm{c}} \\ b_{\mathbf{4}}^{(\alpha)} &= -\zeta \mathbf{E}_2^{(\alpha)} \cdot \mathbf{u}_{\mathrm{c}} \\ b_{\mathbf{5}}^{(\alpha)} &= \zeta \mathbf{E}_1^{(\alpha)} \cdot \mathbf{u}_{\mathrm{c}} \end{aligned}$$

We can get the solution of the curved beam which minimizes $\mathcal{E}$ by solving the Eq.(6.52)

Plate

When a shell is a plate and the potion vector, $\overline{\mathbf{X}}$, moves on a plate, we just use the following equations instead of Eq.(6.51).

$$g_{ij}^{(\alpha\beta)} = \begin{cases} 1 & (i=j) \\ 0 & (i\neq j). \end{cases} \quad \left(\because \mathbf{E}_i^{(\alpha)} = \mathbf{E}_i^{(\beta)}\right) \tag{6.53}$$

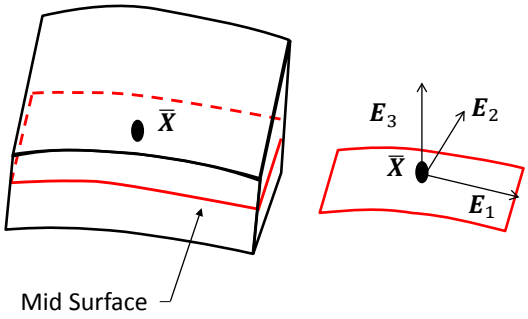

Figure 6.4: Coordinate system and position vector of curved shell

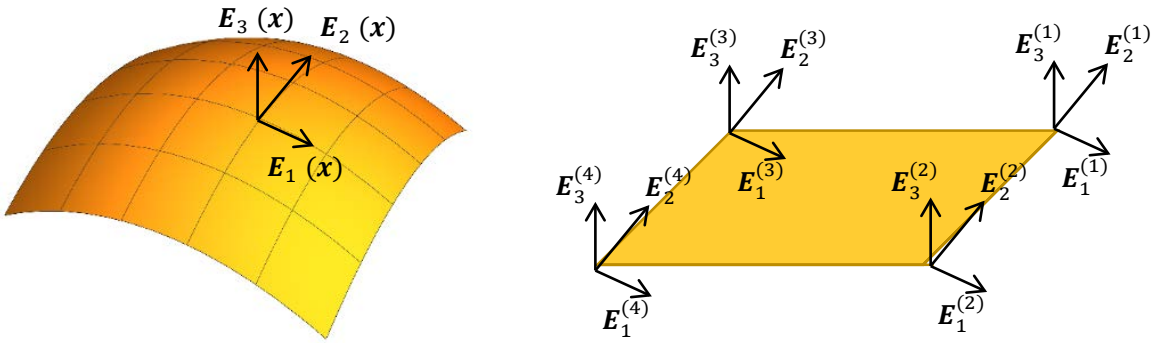

Figure 6.5: Shell element

6.4 Numerical test

In this section, we did the numerical test and evaluated the accuracy of the proposed method. Fig.6.6 shows the procedure of the conversion method. We emphasize that structure element is constructed in the specified domain and don't need to be construct in a full domain. We prepared three solid element models, a cantilever, a slab and a cylinder. All modes are linear

isotropic elastic body. And we also compared the solution of the proposed method with that of the typical method. Appendix A explains the typical conversion method in the numerical test.

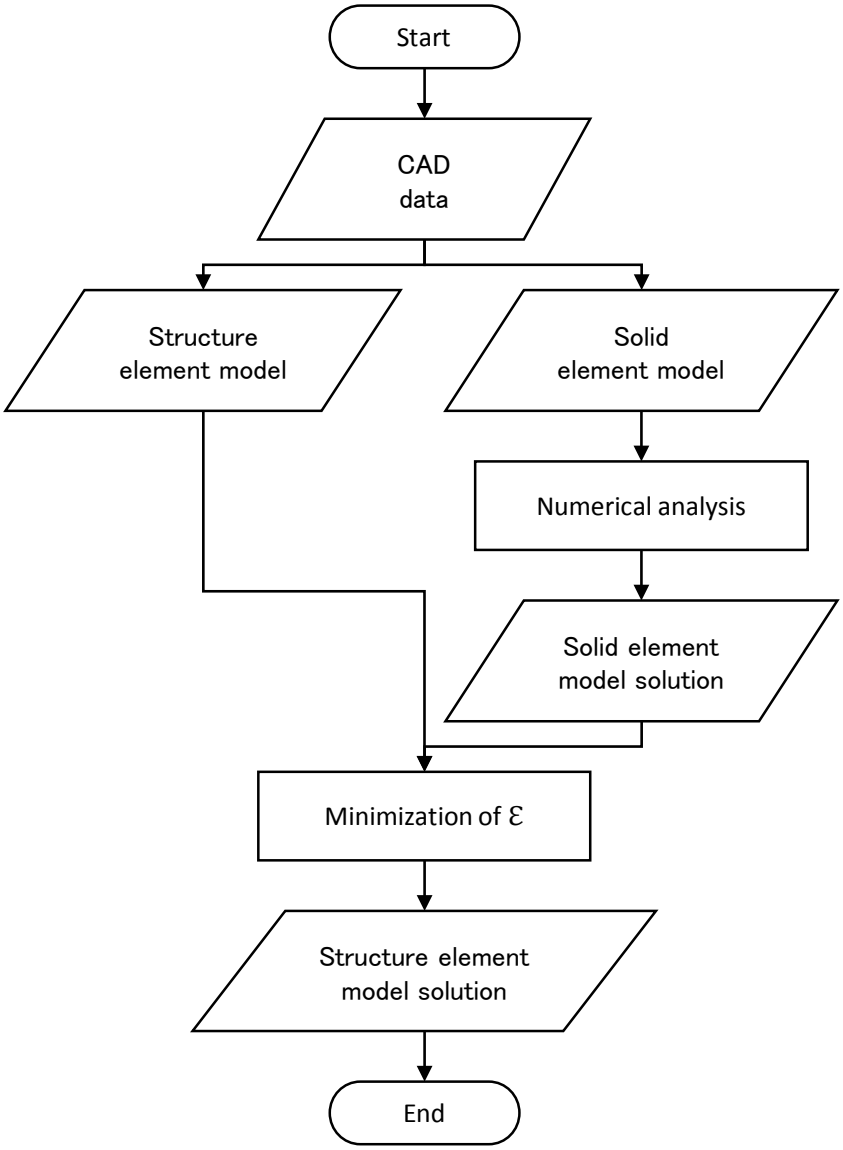

Figure 6.6: Procedure of conversion

6.4.1 Cantilever

We did a static analysis of the cantilever receiving a load to the right end and fixed at the left end. Fig. 6.7 shows the solid model of the cantilever. The solid elements were a quadratic tetrahedral element and minimum length is 10cm. The structure elements were a Timoshenko-

beam passing through the center of the cross section in YZ plane of the solid model.

Fig. 6.8 shows the solution of the solid element model, displacement and stress. There was a disturbance of shear stress at the fixed end. It means that the approximation of a beam model may be not satisfied at the fixed end.

We solved the Eq.(6.37) and got a beam model solution. Fig. 6.9 shows the distance between solid element model solution and beam element model solution respect to a structure element. At the fixed end, there was more than 30 % of a relative error and this error was reduced according to the distance from the fixed end. A reason is that the approximation of a Timoshenko-beam theory is not satisfied at the fixed end as we discussed.

We computed a sectional force, a bending moment and a shear force from the beam model solution. Fig. 6.10 shows a comparison with a sectional force of analytic solution. Except of a shear force at both ends, there was little difference. Adjusting a shear correction factor, k, might make better conversion. Fig. 6.10 shows a comparison with a sectional force of the conventional method. Our proposed method calculated the disturbance at the both ends.

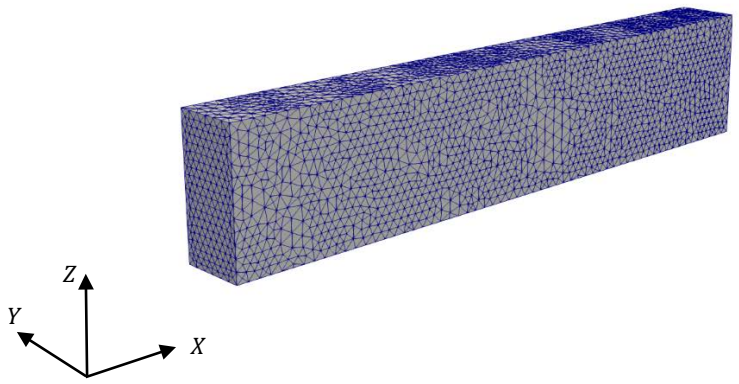

Figure 6.7: Solid model of cantilever (quadratic tetrahedral element)

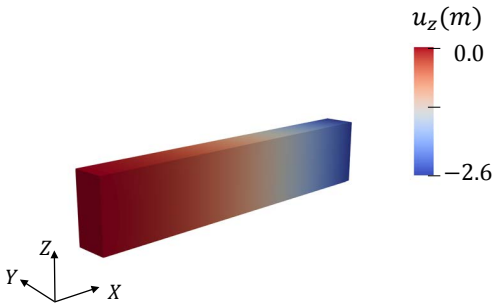

[1] Displacement in z-direction

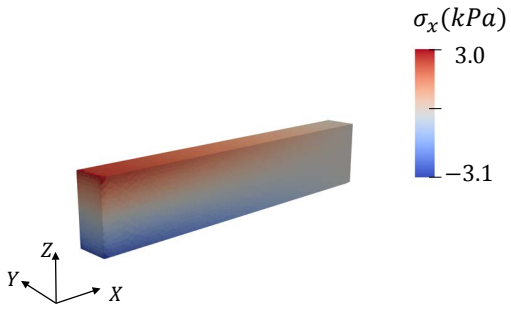

[2] Stress in x-direction

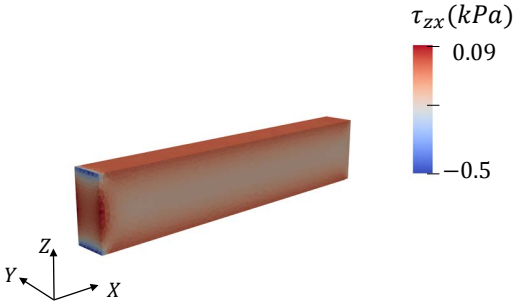

[3] Shear stress in xz direction

Figure 6.8: Numerical solution of the solid model

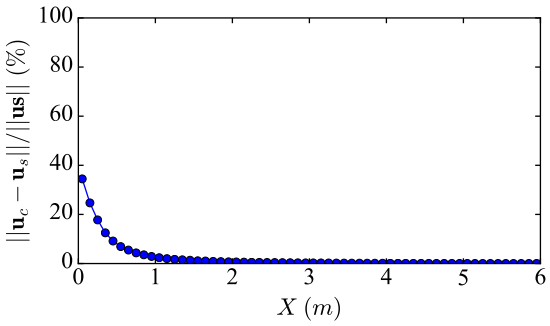

Figure 6.9: Relative error of displacement

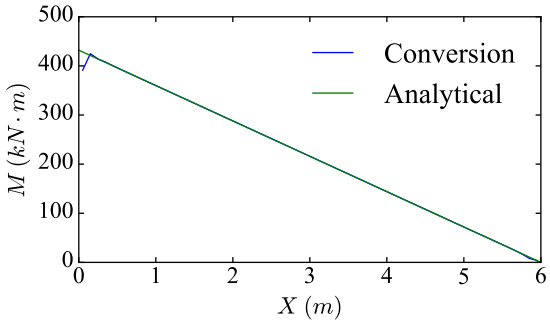

[1]bending moment

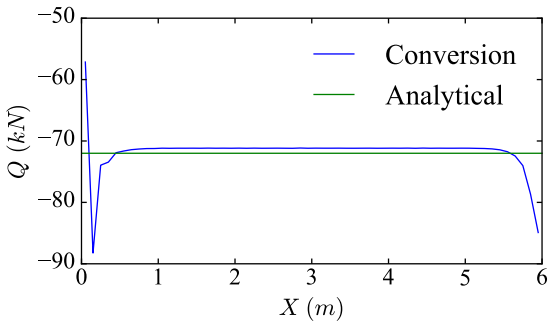

[2]shear force

Figure 6.10: comparison with analysis solution

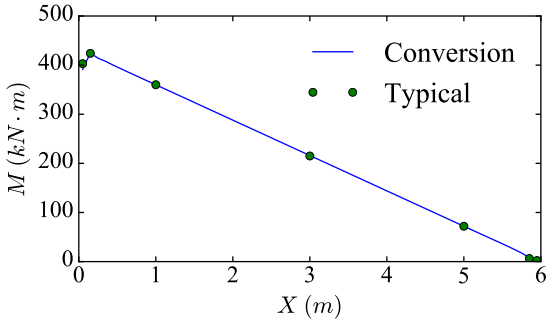

[1]bending moment

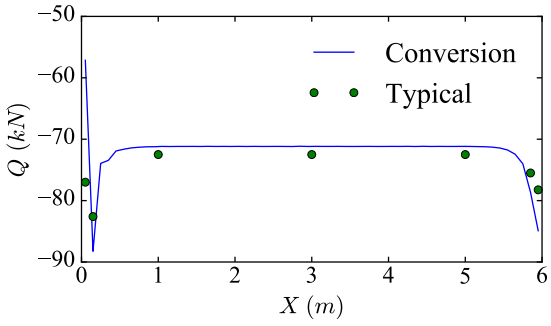

[2]shear force

Figure 6.11: comparison with the conventional method

6.4.2 Slab

We did a static analysis of the slab receiving uniformly distributed load. Fig.6.12 shows the problem settings.

Fig. 6.13 shows the solid element model and the structure element model. The solid elements were a hexahedral element. Structure elements were a quad element of Mindlin–Reissner plate. Two structure element model were located at the edge and the center of the region. We emphasize that all you need to do is to put a structure element model at the region where you want to know a sectional force.

Fig6.14 shows the solid element's solution, displacement and stress. There was a disturbance

of shear stress at the fixed end as the cantilever.

We solved the Eq.(6.52) and got a plate model solution. Fig. 6.15 shows the relative error between solid element model solution and plate element model solution respect to a structure element. As the cantilever, at the fixed end, there was more than 10 % of a relative error and this error was reduced according to the distance from the fixed end. A reason is that the approximation of a Mindlin–Reissner plate theory is not satisfied at the fixed end.

Fig. 6.16 shows a a sectional force of the plate. There was a disturbance at the corner of the model slightly. We should take margins for evaluating regions. We compared this sectional force with those of analytic solution and the conventional method at $Y = 0$ (See Fig. 6.17 and 6.18). Except of at the edge, there was little difference.

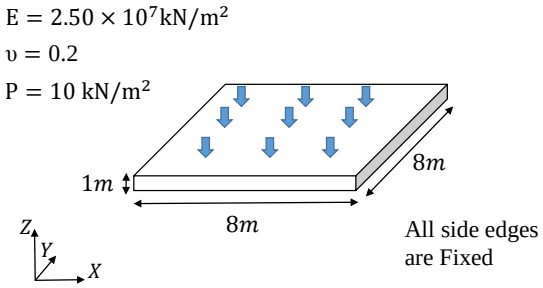

Figure 6.12: Problem settings of slab

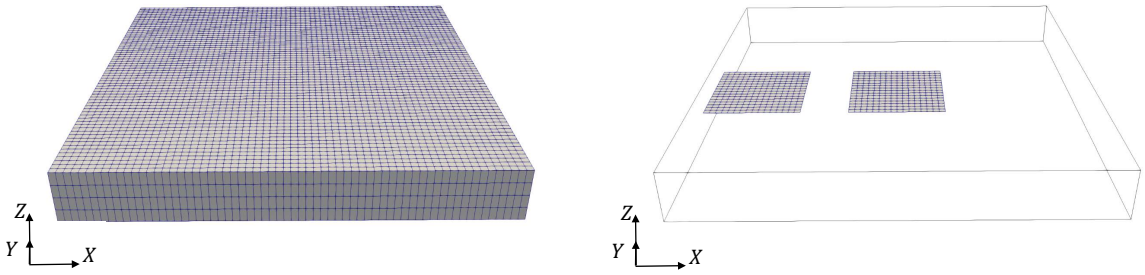

[1] Solid element model [2] Structure element model

Figure 6.13: Model of Slab

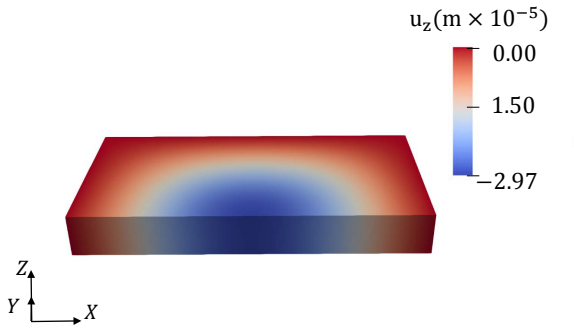

[1] Displacement in z-direction

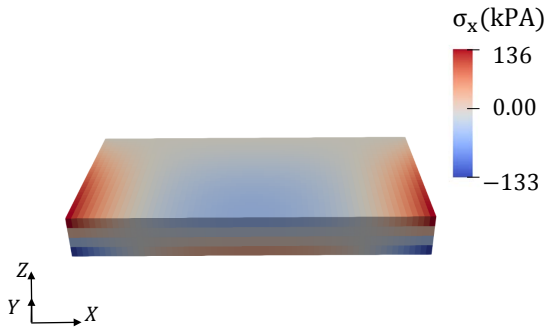

[2] Stress in x-direction

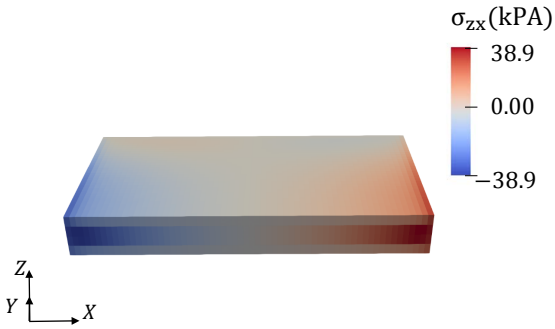

[3] Shear stress in zx-direction

Figure 6.14: Solid element model solution

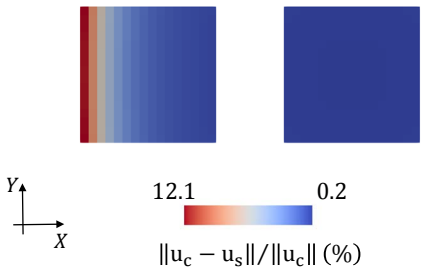

Figure 6.15: Relative error of displacement

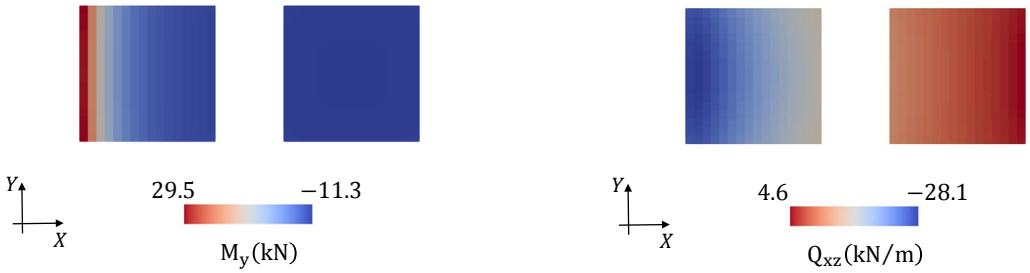

[1] Bending moment [2] Shear force

Figure 6.16: Sectional force

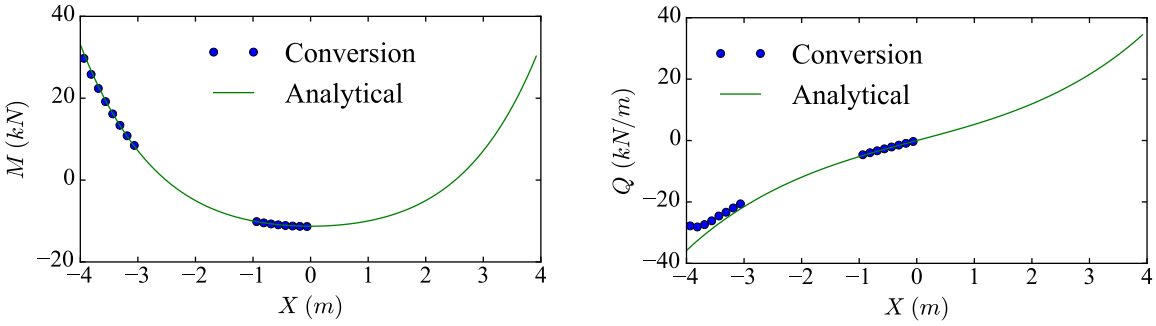

[1] Bending moment [2] Shear force

Figure 6.17: Comparison with the analytic solution ($Y = 0$)

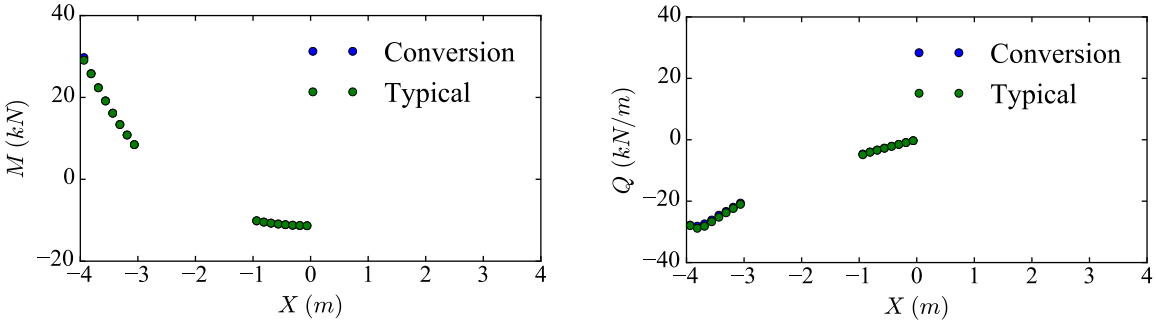

[1] Bending moment [2] Shear force

Figure 6.18: Comparison with the conventional method ($Y = 0$)

6.4.3 Cylinder

We did a static analysis of the cylinder receiving uniformly distributed load along the circular cross-section Fig. 6.19 shows the problem settings. Both edges were fixed.

Fig. 6.20 shows the solid element model and the structure element model. The solid elements were a quadratic tetrahedral element. Structure elements were a quadratic quad element and located at the midsurface.

Fig. 6.21 shows the solution of the solid element model at the cross section where $Z = 0$. The value of norm of displacement and stress in z-direction were the same along circumference. Shear stress was symmetric.

Fig. 6.22 shoes the sectional force of the shell model. It shows the same value along the circumference as the solution of the solid element model. We compared this sectional force with that of the conventional method around $Z = 0$ (See Fig. 6.23). Except of the bending moment near the point where $Z = 0$, there was little difference.

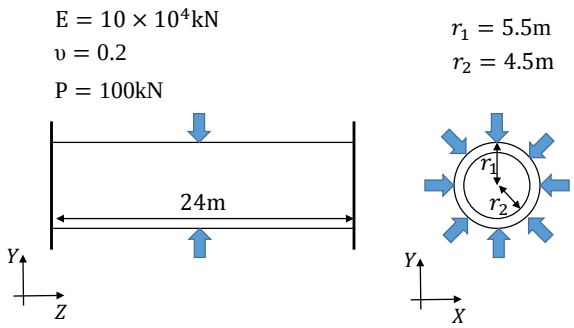

Figure 6.19: Problem settings

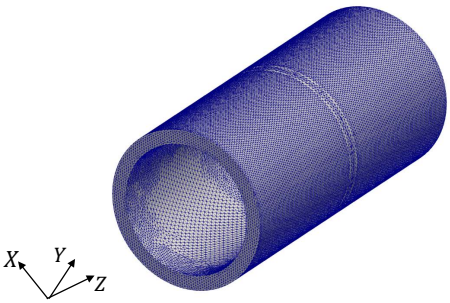

[1]Solid element model

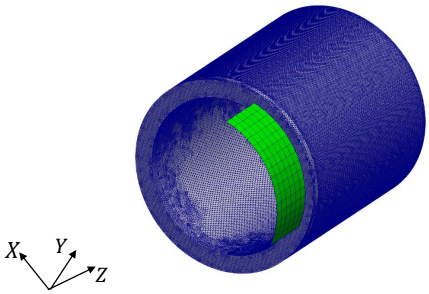

[2]structure element model

Figure 6.20: Model of Cylinder

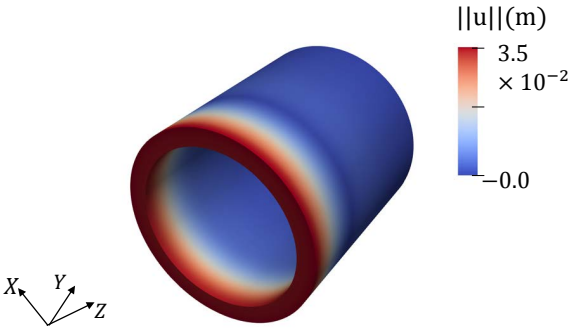

[1] Norm of displacement

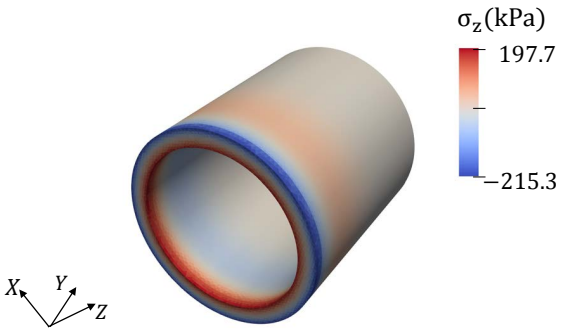

[2] Stress in z-direction

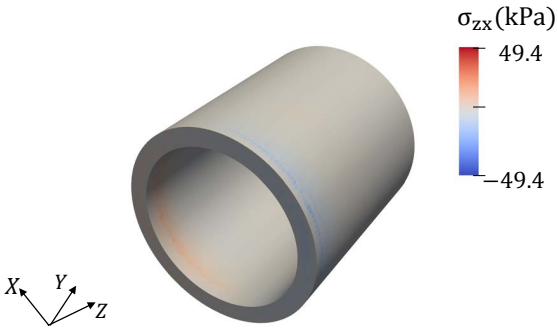

[3] Shear stress in zx-direction

Figure 6.21: Solution of solid element model at the cross section where $Z = 0$

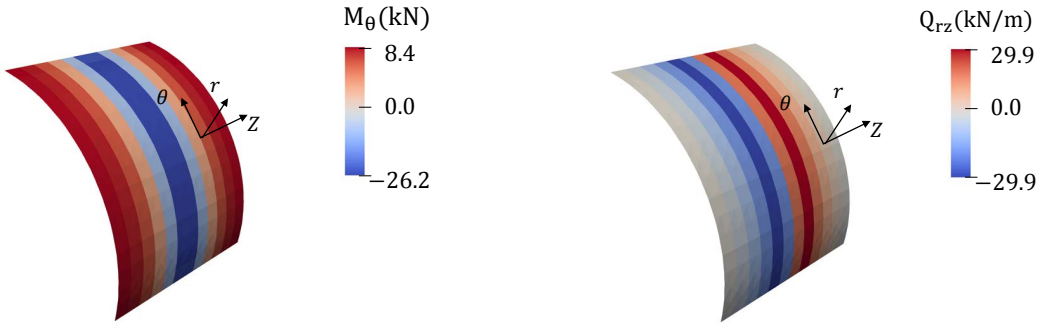

[1] Bending moment [2] Shear force

Figure 6.22: Solution of shell model (Sectional force)

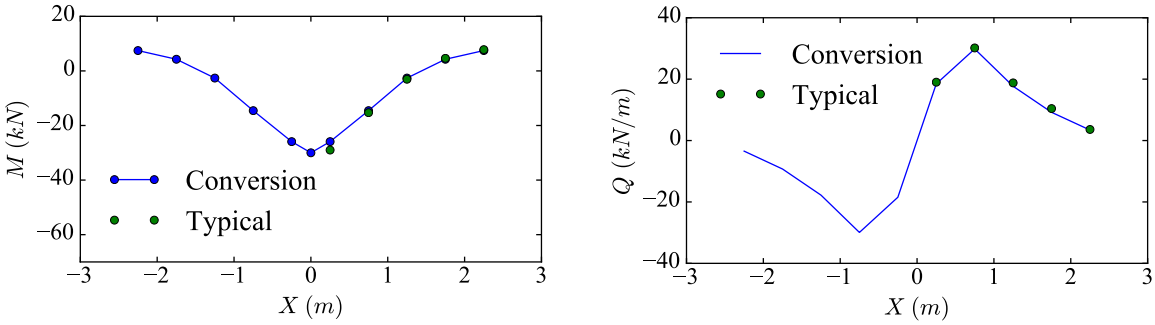

[1] Bending moment [2] Shear force

Figure 6.23: Comparison with a conventional method

6.4.4 Discussion

In all cases, the proposed conversion method showed the capability to compute structure element solutions for specified domain of model with well accuracy. Even at the fixed edge where there is a disturbance of stress, the proposed conversion method was able to reflect this disturbance. The proposed method can compute continuous sectional force for a wide range of domain which can't be done by the typical method.

However there is a little relative error of displacement between solid element and structure element at the fixed edges. It means that the approximation of structure didn't satisfy at these points and there is no guarantee of the equilibrium of forces on this area. One idea for reduction

of the relative error is to minimize the error related to not only to displacement and but also to stress (See Appendix B).

At such points, we should evaluate not only structure element components but also solid element components like displacement and stress. In this viewpoint, computation of the error is important.

6.5 Conclusion

In this chapter, we propose the conversion method from solid element model solutions to structure element model solutions based on the meta-modeling theory. We develop the conversion method for solid element model's solution to curved beam's solution and shell's solution. In all the numerical experiments of a cantilever, a plate and a cylinder, the proposed method converted a solid element model's solution accurately and automatically. With this proposed method, engineers can deal with a numerous amount of solutions of a FEM model of large degree-pf-freedom efficenlty.

Chapter 7

Theoretical analysis of 2D and 3D Multi-spring models

7.1 Introduction

In seismic design, 2D seismic response analysis of soil has been used mainly. To introduce 3D seismic response analysis of soil into seismic design and obtain engineer's approval, comparison of 2D and 3D seismic response analysis is needed. In this viewpoint, comparison of 2D and 3D theory of constitutive relations is beneficial.

As for the constitutive relations that are used in practical geo-technical engineering, we employ multi-spring model (MSM)[23, 24, 44], which is an empirical model based on experiments and has been used for seismic design for a long time. This model consists of a multitude of non-linear 1D shear springs oriented in an arbitrary direction.on one plane (See Figure 7.1). All springs are fixed at the center of the circle and deviation stress tensor $\mathbf{s}$ at this point is computed as the summation of the force of all springs. In the beginning,this model is proposed with plane strain state. And this model is extended to 3D model considering the number of plane

MSM also computes 4-th rank tensor $\mathbf{D}$,which determines the relation of deviation stress tensor $\mathbf{s}$ and strain tensor ϵ in increment form. ($\mathrm{d}\mathbf{s} = \mathbf{D} : \mathrm{d}\epsilon$). There is a difference of $\mathbf{D}$ between 2D MSM and 3D MSM in plane strain state, which prevents the comparison of 2D and 3D

analysis.

The preceding studies[10, 24] shows the difference of solution of 2D and 3D MSM but they lacks of a theoretical analysis for the difference. And another study[35] shows the parameter settings method for MSM which consider the difference of mean stress between 2D and 3D MSM .

However, the difference of **D** is caused not only by the difference of mean stress. Actually,the extension of this model from the two-dimensional setting to the three-dimensional setting is not completed. Unlike preceding studies, we consider reversely, i.e., the reduction from the thee-dimensional setting to the two-dimensional setting, in order to clarify the limitation of the reduction; while the extension from the two-dimensional setting to the three-dimensional setting can be made in an intuitive manner, the reduction from the three-dimensional setting to the two-dimensional can be made most rigorously.

In this section we compare 2D MSM and 3D MSM analytically and numerically and examine a difference of them to clarify the application and limitation of 2D MSM as approximation of 3D MSM. In addition, we propose a parameter setting which eliminate the difference when soil is at safe.

The contents of this section are as follows. First, unified Formulation of 2D and 3D Multi-Spring Models is explain in Subsection 7.2 and we show the difference of 2D MSM and 3D MSM in plain strain state. Then, we examine this difference with MSM with 1D elastic springs in Subsection 7.3. In Subsection 7.4, we review a conventional parameter setting and propose another one which consider the difference. In Subsection 7.5, we did numerical tests and examine the influence of this difference and show application and limitation of 2D MSM as approximation of 3D MSM.

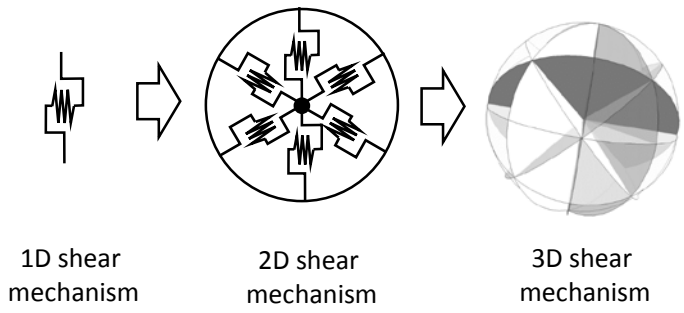

Figure 7.1: Multi-Spring Model

7.2 Unified Formulation of 2D and 3D Multi-Spring Models

In this section, we formulate 2D and 3D MSM and clarify the difference of them and then propose the 2D MSM which is the reduction from the three-dimensional setting.

Constitutive relation in increment form ($\mathrm{d}\sigma = C : \mathrm{d}\epsilon$) can be decomposed of mean stress σ_m and deviation stress $\mathbf{s}$.

$$\mathrm{d}\sigma = \mathrm{d}\sigma_m + \mathrm{d}\mathbf{s} = \mathbf{K} : \mathrm{d}\epsilon + \mathbf{D} : \mathrm{d}\epsilon \tag{7.1}$$

For example, elasticity tensor of isotropic elastic body, $\mathbf{C}^{IE}$, can be decomposed as follows.

$$\begin{aligned}
\mathrm{d}\sigma_{ij} &= C^{IE}_{ijkl}\mathrm{d}\epsilon_{kl} \\
&= \left\{\left(K - \frac{2}{3}G\right)\delta_{ij}\delta_{kl} + G(\delta_{ik}\delta_{jl} + \delta_{il}\delta_{jk})\right\}\mathrm{d}\epsilon_{kl} \\
&= K\delta_{ij}\delta_{kl}\mathrm{d}\epsilon_{kl} + G\left(-\frac{2}{3}\delta_{ij}\delta_{kl} + \delta_{ik}\delta_{jl} + \delta_{il}\delta_{jk}\right)\mathrm{d}\epsilon_{kl}
\end{aligned} \tag{7.2}$$

where K is a bulk module and G is a shear module.

With assumption of plane strain state, equation of (2) can be written in matrix format as follows.

$$\begin{Bmatrix} \sigma_x \\ \sigma_y \\ \tau_{xy} \end{Bmatrix} = K \begin{bmatrix} 1 & 1 & 0 \\ & 1 & 0 \\ sym. & & 0 \end{bmatrix} \begin{Bmatrix} \mathrm{d}\epsilon_x \\ \mathrm{d}\epsilon_y \\ \mathrm{d}\gamma_{xy} \end{Bmatrix} + G \begin{bmatrix} \frac{4}{3} & -\frac{2}{3} & 0 \\ & \frac{4}{3} & 0 \\ sym. & & 1 \end{bmatrix} \begin{Bmatrix} \mathrm{d}\epsilon_x \\ \mathrm{d}\epsilon_y \\ \mathrm{d}\gamma_{xy} \end{Bmatrix} \tag{7.3}$$

MSM computes deviation stress **s** and 4-th rank tensor, **D**.

7.2.1 2D MSM

2D MSM consists of a number of non-linear 1D shear springs oriented in an arbitrary direction on one plane (See Figure 7.2). All springs are fixed at center of unit circle and deviation stress **s** at this point is computed as the summation of force of springs τ.

$$\mathbf{s}_{2D} = \int_0^{2\pi} \tau(\mathbf{d} \otimes \mathbf{t}) \mathrm{d}\psi \tag{7.4}$$

where

τ: force of spring

t: unit tangent vector of spring

d: unit direction vector of spring

ψ: spring angle

Shear strain γ of spring can be computed as follows

$$\gamma^{2D} = \epsilon^{2D} : (\mathbf{d} \otimes \mathbf{t}) \tag{7.5}$$

where ϵ^{2D} is strain tensor in plane strain state and shear stress of spring is a function of γ

$$\tau = f(\gamma) \tag{7.6}$$

where $f(\gamma)$ is a non linear function, i.e., hyperbolic function.

From incremental form of (2), we can drive constitutive relation,

$$\mathrm{d}\mathbf{s}^{2D} = \mathbf{D}^{2D} : \mathrm{d}\epsilon^{2D} \tag{7.7}$$

where

$$\mathbf{D}^{2D} = \int_0^{2\pi} \frac{1}{2} G^{1D}(\gamma^{2D})(\mathbf{d} \otimes \mathbf{t} + \mathbf{t} \otimes \mathbf{d}) \otimes (\mathbf{d} \otimes \mathbf{t} + \mathbf{t} \otimes \mathbf{d}) \mathrm{d}\psi \tag{7.8}$$

$$G^{1D} = \frac{\mathrm{d}f}{\mathrm{d}\gamma} \tag{7.9}$$

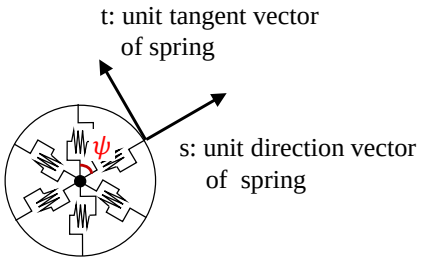

Figure 7.2: 2D Multi-Spring Model

7.2.2 3D MSM

3D MSM consists of a number of planes with 1D shear springs and is the extension of 2D MSM. The unit normal vector of planes **n** can be expressed in sphere coordinate (See Figure 7.3).

$$\mathbf{n}(\phi, \theta) = \{\sin\phi \ \cos\theta, \sin\phi\cos\theta, \cos\phi\}^T \tag{7.10}$$

Deviation stress at the center of sphere is computed by triple integration,

$$\mathbf{s}^{3D} = \int_0^{2\pi}\int_0^{\pi}\left(\int_0^{2\pi} f(\gamma^{3D})(\mathbf{d}\otimes\mathbf{t})\mathrm{d}\psi\right)\sin\phi\ \mathrm{d}\phi\mathrm{d}\theta \tag{7.11}$$

where $\gamma^{3D} = \epsilon^{3D} : (\mathbf{d}\otimes\mathbf{t})$ and ϵ_{3D} is strain tensor in three dimension.

From incremental form of (6), we can drive constitutive relation,

$$\mathrm{d}\mathbf{s}^{3D} = \mathbf{D}^{3D} : \mathrm{d}\epsilon^{3D}$$

where

$$\mathbf{D}^{3D} = \frac{1}{2}\int_0^{2\pi}\int_0^{\pi}\left(\int_0^{2\pi} \mathrm{G}^{1D}(\gamma^{3D})(\mathrm{d}\otimes\mathrm{t}+\mathrm{t}\otimes\mathrm{d})\otimes(\mathrm{d}\otimes\mathrm{t}+\mathrm{t}\otimes\mathrm{d})\mathrm{d}\psi\right)\sin\phi\ \mathrm{d}\phi\mathrm{d}\theta \tag{7.12}$$

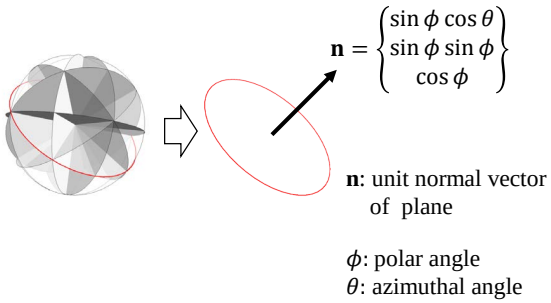

Figure 7.3: Normal vector of plane

7.2.3 Comparsion of 2D and 3D MSM

From equation of (13) with the assumption of plain strain state ($\epsilon^{3D} \rightarrow \epsilon^{2D}$) , we can derive $\overline{\mathbf{D}}^{3D}$, which is $\mathbf{D}^{3D}$ in plane strain state,

$$\overline{\mathbf{D}}^{3D} = \frac{1}{2}\int_0^{2\pi}\int_0^{\pi}\left(\int_0^{2\pi} \mathrm{G}^{1D}(\gamma^{2D})(\mathrm{d}\otimes\mathrm{t}+\mathrm{t}\otimes\mathrm{d})\otimes(\mathrm{d}\otimes\mathrm{t}+\mathrm{t}\otimes\mathrm{d})\mathrm{d}\psi\right)\sin\phi\ \mathrm{d}\phi\mathrm{d}\theta \qquad (7.13)$$

It is clear that $\overline{\mathbf{D}}^{3D}$ in plain strain state is not the same as $\mathbf{D}^{2D}$. We need more assumption that θ, ϕ is constant to get the $\mathbf{D}^{2D}$. This assumption means that 2D MSM reduces a number of plane to one plane and ignores the contribution of the springs out out of the plane.Figure 7.4 shows reduction from 3D MSM to 2D MSM. We must pay attention for this difference to compare 2D MSM and 3D MSM.

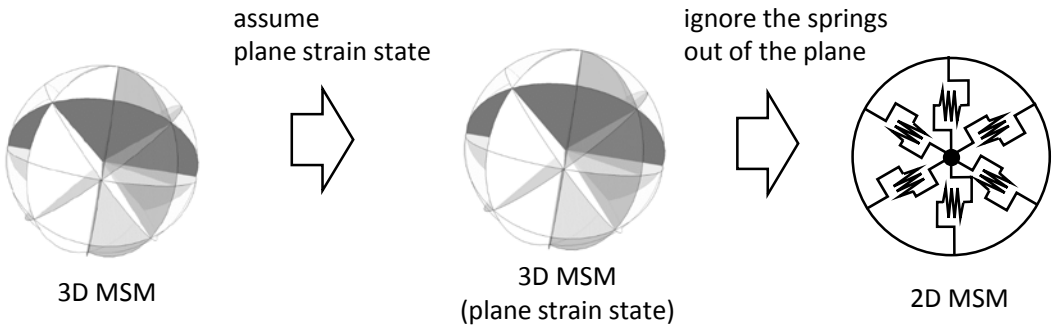

Figure 7.4: reduction from 3D MSM to 2D MSM

7.3 Comparison with elastic 1D spring

We calculate $\mathbf{D}^{2D}$ and $\mathbf{D}^{3D}$ in plane strain state with elastic springs to examine the difference between them. In this case, G_{1D} is constant.

7.3.1 2D MSM

When we determine two unit vector $\mathbf{e}_1$ and $\mathbf{e}_2$ which are orthogonal, $\mathbf{d}$ and $\mathbf{t}$ can be computed as below.

$$\begin{aligned} \mathbf{d}(\psi) &= \cos\psi\ \mathbf{e}_1\ + \sin\psi\ \mathbf{e}_2 \\ \mathbf{t}(\psi) &= -\sin\psi\ \mathbf{e}_1\ + \cos\psi\ \mathbf{e}_2 \end{aligned} \tag{7.14}$$

where

$$\mathbf{e}_1 = \{1, 0\}^T$$

$$\mathbf{e}_2 = \{0, 1\}^T$$

Substituting equation of (12) and (13) into equation of (6), we can derive $\mathbf{D}^{2D}$ in matrix format[46].

$$\mathbf{D}^{2D} = G^{2D} \begin{bmatrix} 1 & -1 & 0 \\ & 1 & 0 \\ sym. & & 1 \end{bmatrix} \tag{7.15}$$

where $G^{2D} = D_{33}^{2D}$.

7.3.2 3D MSM

$\mathbf{e}_1$ and $\mathbf{e}_2$ on the plane with the normal vector $\mathbf{n}$ (ϕ, θ) can be computed by the two rotation matrix, $R_1(\theta)$ and $R_2(\theta, \phi)$ using the right-hand rule.

$$\mathbf{e}_1(\phi, \theta) = \mathbf{R}_2(\phi, \theta)\mathbf{R}_1(\theta)\mathbf{e}_x$$

$$\mathbf{e}_2(\phi, \theta) = \mathbf{e}_1 \times \mathbf{n}$$

where $\mathbf{e}_x = \{1, 0, 0\}^T$.

d and **t** can be computed as below.

$$\mathbf{d}(\phi, \theta, \psi) = \cos\psi\ \mathbf{e}_1\ + \sin\psi\ \mathbf{e}_2$$

$$\mathbf{t}(\phi, \theta, \psi) = \mathbf{d} \times \mathbf{n}$$

Substituting equation of them into equation of (6), we can derive $\overline{\mathbf{D}}_{3D}$ (=$\mathbf{D}_{3D}$ in plane strain state) in matrix format.

$$\overline{\mathbf{D}}^{3D} = G^{3D} \begin{bmatrix} \frac{4}{3} & -\frac{2}{3} & 0 \\ & \frac{4}{3} & 0 \\ sym. & & 1 \end{bmatrix}$$

where $G^{3D} = \overline{D}_{33}^{3D}$. $\overline{\mathbf{D}}^{3D}$ is the same as Isotropic elastic one's.

7.3.3 Comparsion of 2D MSM and 3D MSM

Difference of coefficient matrix of $\mathbf{D}^{2D}$ and $\overline{\mathbf{D}}^{3D}$ means $\mathbf{D}^{2D}$ can't be consistent with $\overline{\mathbf{D}}^{3D}$ even if parameters for 2D MSM are adjusted to 3D MSM.

With the assumption of $G = D_{33}^{2D} = \overline{D}_{33}^{3D}$, the difference between $\mathbf{D}^{2D}$ and $\overline{\mathbf{D}}^{3D}$ is

$$\overline{\mathbf{D}}^{\mathbf{3D}} - \mathbf{D}^{2D} = \frac{G}{3} \begin{bmatrix} 1 & 1 & 0 \\ 1 & 1 & 0 \\ 0 & 0 & 0 \end{bmatrix} \tag{7.16}$$

This difference suggests that 2D MSM is a good approximating of 3D MSM for shear deformation, but there is difference between them for volume deformation.

Although there is a difference of **D**, it is possible to make consistency of 4-th tensor, **C** by adjusting parameter of 4-Th tensor, **K** in case of MSM with elastic springs.

$$\mathrm{d}\sigma = \mathrm{d}\sigma_m + \mathrm{d}\mathbf{s} = (\mathbf{K} + \mathbf{D}) : \mathrm{d}\epsilon = \mathbf{C} : \mathrm{d}\epsilon \tag{7.17}$$

In plain strain state, 4-Th tensor,**K** ,can be written in matrix format as follows.

$$\mathbf{K} = K\begin{bmatrix} 1 & 1 & 0 \\ 1 & 1 & 0 \\ 0 & 0 & 0 \end{bmatrix}$$

where K is a bulk modules. This coefficient matrix of **K** is the same as one of the Eq. (21). Therefore we can eliminate the difference of **D** by using different parameter of K. For example, if we use $K^{2D} = K + \frac{G}{3}$, then

$$\begin{aligned} \mathbf{C}^{2D} &= \mathbf{K}^{2D} + \mathbf{D}^{2D} \\ &= \left(K + \frac{G}{3}\right)\begin{bmatrix} 1 & 1 & 0 \\ 1 & 1 & 0 \\ 0 & 0 & 0 \end{bmatrix} + G\begin{bmatrix} 1 & -1 & 0 \\ -1 & 1 & 0 \\ 0 & 0 & 1 \end{bmatrix} \\ &= K^{3D}\begin{bmatrix} 1 & 1 & 0 \\ 1 & 1 & 0 \\ 0 & 0 & 0 \end{bmatrix} + G\begin{bmatrix} \frac{4}{3} & -\frac{2}{3} & 0 \\ -\frac{2}{3} & \frac{4}{3} & 0 \\ 0 & 0 & 1 \end{bmatrix} \\ &= \overline{\mathbf{C}}^{3D} \end{aligned} \tag{7.18}$$

where $\overline{\mathbf{C}}^{3D} = \mathbf{K} + \overline{\mathbf{D}}^{3D}$.

We must mention that this method is only applicable with MSM with elastic springs. In MSM with inelastic springs, **D** changes along with shear deformation and this consistency of **C** is broken.

7.4 Parameter setting method

In this section,we review parameter setting method for 2D and 3D MSM and then propose new parameter setting method considering the difference of **D**.

7.4.1 Input parameter

A hyperbolic function, $f(\gamma)$, which express relation of shear stress and strain of MSM's springs is a function of initial shear modules,G_0, and shear strength, τ_f,

$$\tau = f(\gamma) = f(\gamma, G_0, \tau_f) \tag{7.19}$$

G_0 is the function of mean stress, σ_m,

$$G_0 = G_{ma}\sqrt{\frac{\sigma_m}{\sigma_{ma}}}$$

where G_{ma} is initial shear modules when $\sigma_m = \sigma_{ma}$, and called as "reference elastic shear modules".

τ_f is calculated by Mohr–Coulomb failure criterion,

$$\tau_f = \frac{\sigma_3 + \sigma_1}{2}\sin\phi_f$$

where σ_3, σ_1 are principal stress and ϕ_f is shear resistance angle

Bulk modules,K, is also a function of mean stress,

$$K = K_{ma}\sqrt{\frac{\sigma_m}{\sigma_{ma}}}$$

where K_{ma} is Bulk modules when $\sigma_m = \sigma_{ma}$, and called as "reference elastic bulk modules".

So Input parameter for MSM are G_{ma}, K_{ma}, σ_{ma} and ϕ_f (Table 7.1).

Table 7.1: Input Parameter for MSM

K_{ma}	reference elastic bulk modules
G_{ma}	reference elastic shear modules
σ_{ma}	reference confining pressure
ϕ_f	shear resistance angle

7.4.2 Conventional method[35]

These input parameters are determined to match observation data of shear stiffness of soil at rest.

G_{ma} is determined by V_s which is observed by PS logging,

$$G_{ma} = \rho V_s$$

where ρ is density.

K_{ma} is computed as follows,

$$K_{ma} = \frac{1}{3(2-\nu)} \frac{2}{1+\nu} G_{ma}$$

where ν is poisson ratio.

Reference confining pressure is, σ_{ma}, is determined by the vertical pressure, σ_v , and horizontal pressure , σ_h , at the center depth of soil unit,

$$\sigma_{ma} = \frac{\sigma_v + \sigma_h + \sigma_h}{3} = \frac{1+2K_0}{3}\sigma_v \quad (\because \sigma_h = K_0 \sigma_v)$$

where K_0 is at-rest earth pressures.

However, in 2D MSM , mean stress is computed as follows,

$$\sigma_m^{2D} = \frac{\sigma_x + \sigma_z}{2}$$

So σ_{ma}^{2D} is determined as follows,

$$\sigma_{ma}^{2D} = \frac{\sigma_v + \sigma_h}{2} = \frac{1+K_0}{2}\sigma_v$$

Shear resistance angle is determined by a triaxial test with drain condition or a repeat triaxial test.

7.4.3 Proposed method

Conventional method which considers only the difference of mean stress can match observation data of shear stiffness of soil at rest. However, as we discussed, even if shear stiffness is the same of 2D and 3D MSM, there is a still deference of **D**.

From Eq.(24), we propose new parameter setting for K_{ma} of 2D MSM as follows,

$$K_{ma}^{2D} = \frac{1}{3(2-\nu)}\frac{2}{1+\nu}G_{ma} + \frac{1}{3}G_{ma}$$

As we mentioned , this parameter setting is applicable only for MSM without or with Small shear deformation like soil at rest.

7.5 Numerical experiments

We did numerical experiments to compare stress-strain relation of 2D MSM and 3D MSM with conventional and proposed parameter settings. We use the material parameters which was shown in the proceeding study[10].

We did two tests, K_0 compression and simple Shear test plain strain state. In K_0 compression, vertical load is applied to soil with horizontal displacement constraint. After K_0 compression, shear stress is applied by quasi-static analysis (Fig. 7.5) in drained and undrained case.

We use input parameters which are used in preceding studies (Table 7.2). Parameters for 2D MSM are adjusted according to conventional and proposed parameter settings.

In this experiment, we treat the direction of compression as positive.

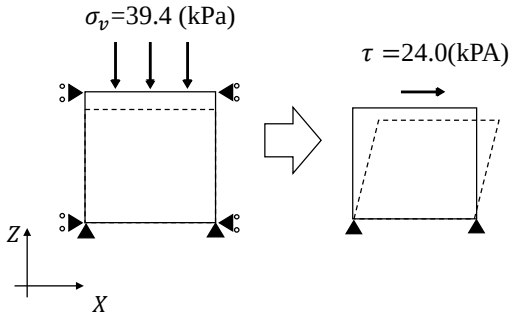

Figure 7.5: K_0 compression and Simple Shear Test

Table 7.2: Input parameter for MSM

	ρ (t/m^3)	G_{ma} (kPA)	K_{ma} (kPA)	σ_{ma} (kPA)	ϕ_f (deg)	h_{max}
MSM2D (Conventional)	2.0	18170	47385	29.8	43.5	0.24
MSM2D (Proposed)	2.0	18170	50385	29.8	43.5	0.24
MSM3D	2.0	18170	47385	26.5	43.5	0.24

7.5.1 K_0 compression

Fig.7.6 shows stress and strain relation and Table7.3 shows parameters when compression is finished . In comparison with 2D MSM of conventional method and 3D MSM, the difference of initial shear modules, G_0 is small, but the difference of vertical strain,ϵ_z, is large. This difference is caused because 2D MSM ignores the contribution of the springs out out of the plane as we discussed. On the other hand , 2D MSM of proposed method has the same stress-strain relation as one of 3D MSM.

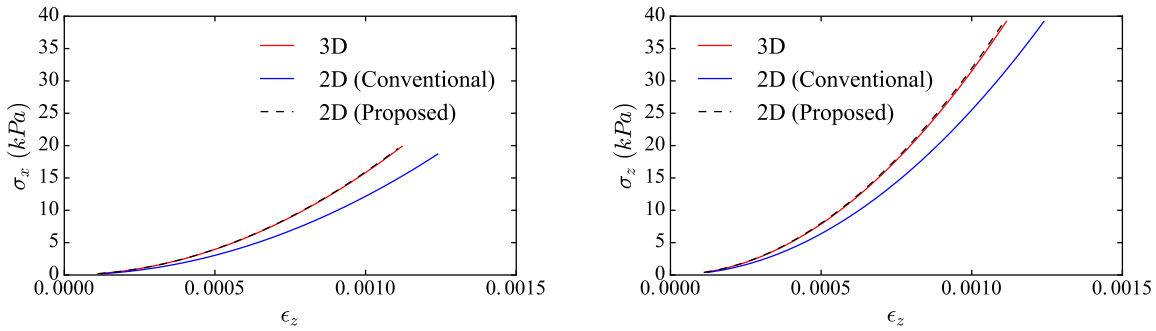

[1] $\sigma_x - \epsilon_z$ [2] $\sigma_z - \epsilon_z$

Figure 7.6: Stress and strain of K_0 Compression

Table 7.3: Comparison of K_0 Compression

	ϵ_z	σ_x (kPa)	σ_z (kPa)	G_0 (kPa)
MSM2D (Conventional)	0.0012	18.7	39.2	17961
MSM2D (Proposed)	0.0011	19.6	39.2	18095
MSM3D	0.0011	19.9	39.2	18172

7.5.2 Simple shear test in drained case

In drained case, with shear deformation, **D** becomes small and vertical strain is compressed to sustain σ_z so that horizontal stress, σ_x, increases.

Fig. 7.7 shows stress and strain relation. The difference of shear stress-strain relation is small. But there is the difference of ϵ_z.

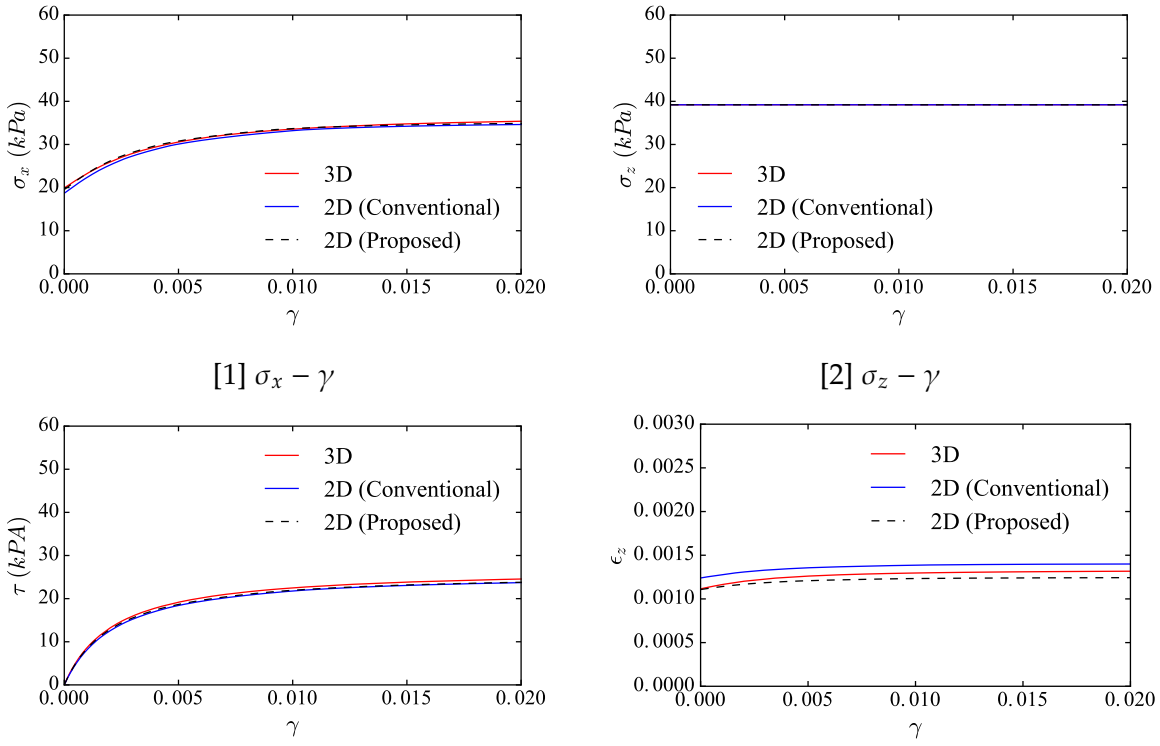

[1] $\sigma_x - \gamma$ [2] $\sigma_z - \gamma$

[3] $\tau - \gamma$ [4] $\epsilon_z - \gamma$

Figure 7.7: Stress and strain of of simple shear test (drained case)

Table 7.4: Comparison of simple shear test (drained case)

	γ	ϵ_z	σ_x (kPa)	σ_z (kPa)	τ (kPA)
MSM2D (Conventional)	0.02	0.0014	34.4	39.2	23.3
MSM2D (Proposed)	0.02	0.0012	34.9	39.2	23.8
MSM3D	0.02	0.0013	35.4	39.2	24.5

7.5.3 Simple shear test in undrained case

In undrained case, with shear deformation, **D** becomes small and pore water pressure become large instead of the compression of vertical strain. In this case, the vertical stress changes along with the change of **D**.

Fig. 7.8 shows the change of stress and strain. There is a difference of vertical stress because of the difference of the coefficient matrix of **D**. In addition, while mean of maximum and minimum principal stress is constant in 2D MSM, this value decreases in 3D MSM. See Appendix for the reason of this value is constant in 2D MSM. Shear strength is calculated by mean of maximum and minimum principal so that there is a difference of the shear stress-strain relation between 2D and 3D MSM.

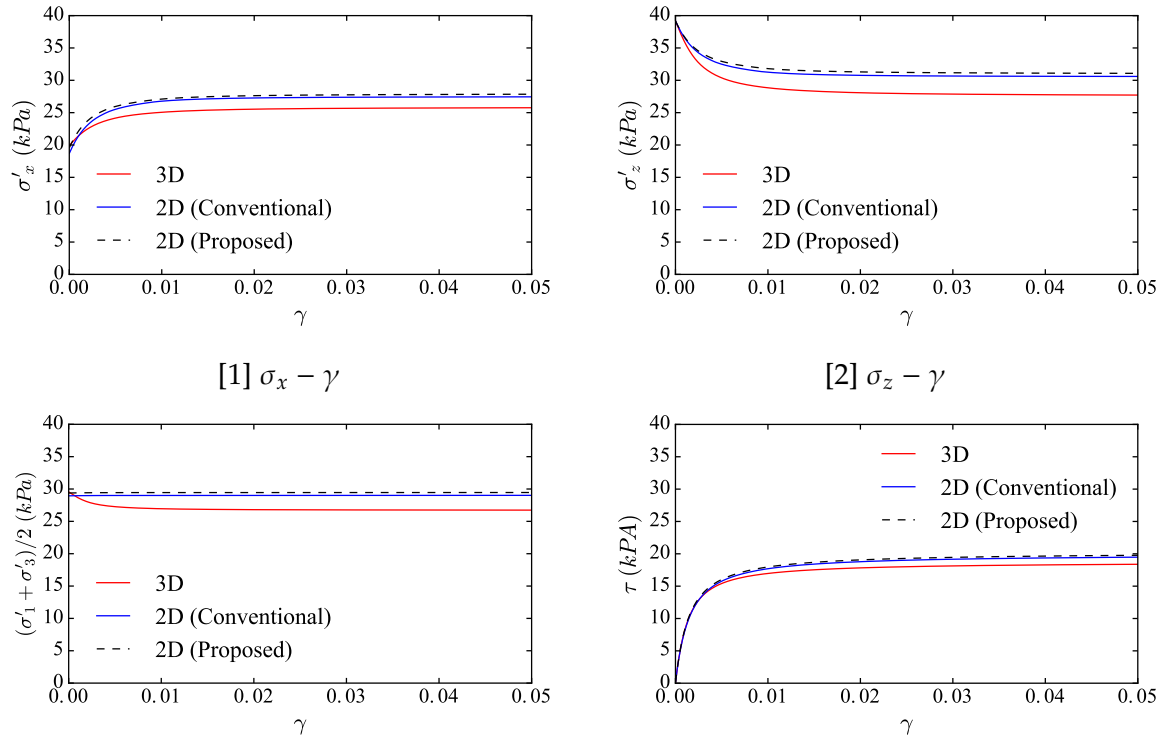

[1] $\sigma_x - \gamma$ [2] $\sigma_z - \gamma$

[3] Principal stress-γ [4] $\tau - \gamma$

Figure 7.8: Stress and strain of of simple shear test (undrained case)

Table 7.5: Comparison of simple shear test (undrained case)

	γ	σ_x (kPA)	σ_z (kPa)	$(\sigma_1 + \sigma_3)/2$ (kPa)	τ (kPa)
MSM2D (Conventional)	0.05	27.5	30.5	29.0	19.5
MSM2D (Proposed)	0.05	27.8	31.0	29.4	20.0
MSM3D	0.05	25.8	27.7	26.8	18.4

7.5.4 Discussion

By adjusting parameter according to the proposed method, 2D MSM has the same stress-strain relation as one of 3D MSM in K_0 compression. In this case, shear strain deformation is small so that our proposed method is applicable.

In simple shear test with drained analysis, the influence of the difference of **D** is small because vertical stress is fixed.There is little difference of stress-strain relation.

However, in simple shear test with undrained analysis, vertical stress is unfixed and that the difference of the coefficient matrix of **D** makes the difference of σ_x and σ_z and shear strength. In addition, there is the difference of shear stress-strain relation because of shear strength when shear strain is larger than 0.5%. Adjustment of shear strength is needed to eliminate this difference.

7.6 Conclusion

In this section, we do theoretical analysis of 2D and 3D MSM and clarify the differences of them. There is a difference of stress-strain relation between 2D MSM and 3D MSM in plain strain state because 2D MSM ignores the contribution of the springs out out of the plane. Although 2D MSM has similar characteristics to 3D MSM, we shouldn't regard 2D MSM as 3D MSM in plain strain state.

This difference suggests that we should use different input parameters for 2D and 3D MSM to match empirical tests. We propose a parameter setting for 2D and 3D MSM considering this difference. This method makes this difference little. But it is only applicable for soil with small share deformation less than 0.5 %. With more share deformation, the influence of difference

become larger and it is difficult to eliminate this difference. This is the limitation of 2D MSM as approximation of 3D MSM.

Chapter 8

Concluding Remarks

For the utilization of HPC-FEM in the practical geo-tech field, coordinated improvements of HPC-FEM components, pre-process, solver, post-processing and theory are needed. In this viewpoint, this dissertation solved the three major limitations of HPC-FEM. These are related to solver, post-processing and theory.

First of all, we implement a HPC-FEM technique into an existing FEM program which has been used in practice and examined the the performance of it compared with the direct solver for matrix equations of the geo-tech field. The CG method was 50 times faster than the direct method with the FEM model which consists in liquefaction layers of soil and structures with an appropriate preprocess matrix. Applicability of the CG method for the geo-tech field is confirmed. In addition, this result shows possibility of re-utilizing FEM programs used in practice with HPC environment

As for the solver, we fixed the ill behavior of solution in liquefaction analysis for the quality assurance of numerical analysis. Through some numerical experiments, we found that there can be a disturbance of solution at the interface of soil and structure because of numerical errors. We developed the HPC-FEM that uses quadruple precision, so that most of numerical errors are suppressed. This solver can be a verification tool for codes.

As for the post-processing, we propose the efficient conversion method from a three-dimensional solid element model solution to a structure element model solution like sectional

force. The physical background which guarantee the consistency between the solid and structure element solution is supported by meta-modeling theory. Through the numerical experiments, the proposed method showed the capability to compute structure element solutions for a wide range of domain with well accuracy and efficiency. This conversion helps engineers to interpret an enormous numerical results of three dimensional analysis.

As for the theory, we do theoretical analysis of 2D and 3D multi-spring model and clarify the differences of them. There is a difference of stress-strain relation between 2D MSM and 3D multi-spring model in plain strain state because 2D MSM ignores the contribution of the springs out out of the plane. Although 2D MSM has similar characteristics to 3D MSM, we shouldn't regard 2D MSM as 3D MSM in plain strain state. We did some numerical analysis and examine the differences numerically. Using different input parameter can reduce the influence of this difference bu can't eliminate it completely when a shear deform is large. We must pay attention this difference.

Appendix A

Typical conversion method

The procedure of a typical conversion method is showed as follows: 1) Evaluation of point data on the specified cross section. 2) Constriction of an approximated function by linear or curve regression. 3) Interpolation of the approximated function. This method constructs a linear function, $LF(x)$, by a regression of vertical stress, σ and compute bend moment, M:

$$M = \int LF(x)x\mathrm{d}x \tag{A.1}$$

This method constructs a quadratic function,$QF(x)$, by a regression of shear stress, σ and compute shear force, Q:

$$Q = \int QF(x)\mathrm{d}x \tag{A.2}$$

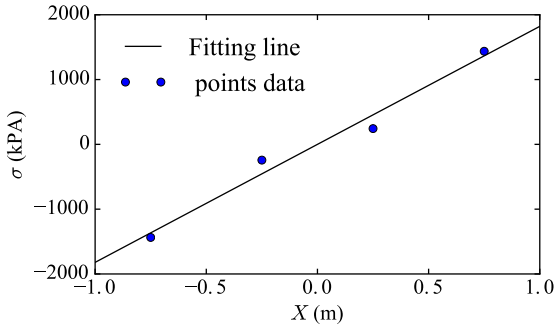

[1] Liner regression for bending moment

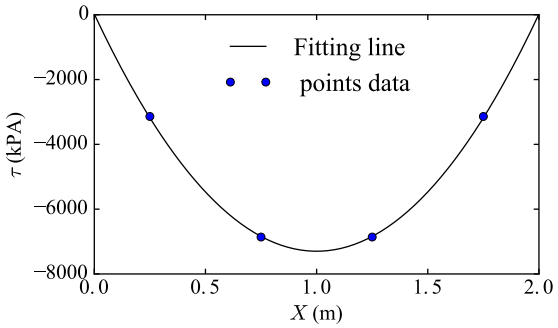

[2] Curve regression for shear force

Figure A.1: Linear or curve regression

Appendix B

Minimization of error of stress

In order to relate a solution of a solid element, we can define another error function $\mathcal{E}'$ with stress tensor σ ,

$$\mathcal{E}' = \int |\sigma^c - \sigma^s|^2 \, \mathrm{d}V = \int \sum_{p,q} \left(\sigma^c_{pq} - \sigma^s_{pq}\right)^2 \, \mathrm{d}V \quad , \tag{B.1}$$

σ^c and σ^s are stress tensor of solid element model and structure element model.

With unit orthonormal vectors $\{\mathbf{E}_1(\mathbf{x}),\ \mathbf{E}_2(\mathbf{x}),\ \mathbf{E}_3(\mathbf{x})\}$ on the midsurface of a shell, vector and tensor can be written as below,

$$\mathbf{x} = \mathbf{X}_i \mathbf{E}_i, \tag{B.2}$$

$$\sigma = \sigma_{ij} \mathbf{E}_i \otimes \mathbf{E}_j, \tag{B.3}$$

$$\epsilon = \epsilon_{ij} \mathbf{E}_i \otimes \mathbf{E}_j, \tag{B.4}$$

$$\sigma_{ij} = C_{ijkl} \epsilon_{kl}, \tag{B.5}$$

C_{ijkl} is a fourth order elastic stiffness tensor component of a plate.

And strain component can be written as below,

$$\epsilon_{ij} = \frac{1}{2}\left(\frac{\partial \mathbf{u} \cdot \mathbf{E}_i}{\partial X_j} + \frac{\partial \mathbf{u} \cdot \mathbf{E}_j}{\partial X_i}\right) = \frac{1}{2}\left(\frac{\partial \mathbf{u}}{\partial X_j} \cdot \mathbf{E}_i + \frac{\partial \mathbf{u}}{\partial X_i} \cdot \mathbf{E}_j\right). \tag{B.6}$$

Substituting Eq.(6.42), we can derive

$$\epsilon_{ij}^{S} = \frac{1}{2}\sum\left(U_k^{(\alpha)}P_{ijk}^{(\alpha)} + \zeta\Theta_2^{(\alpha)}P_{ij1}^{(\alpha)} - \zeta\Theta_1^{(\alpha)}P_{ij2}^{(\alpha)}\right), \tag{B.7}$$

$$\sigma_{pq}^{S} = C_{pqrs}\epsilon_{rs}^{S} = \frac{1}{2}C_{pqrs}\sum\left(U_k^{(\alpha)}P_{ijk}^{(\alpha)} + \zeta\Theta_2^{(\alpha)}P_{ij1}^{(\alpha)} - \zeta\Theta_1^{(\alpha)}P_{ij2}^{(\alpha)}\right), \tag{B.8}$$

where

$$P_{ijk}^{(\alpha)} = \left(\frac{\partial N^{(\alpha)}}{\partial X_j}\mathbf{E}_i + \frac{\partial N^{(\alpha)}}{\partial X_i}\mathbf{E}_j\right)\cdot\mathbf{E}_k^{(\alpha)}.$$

We compute the partial derivative of $\mathcal{E}'$ with respect to $\overline{U}_i^{(\alpha)}$ and $\Theta_i^{(\alpha)}$ which are unknown values,

$$\frac{\partial\mathcal{E}'}{\partial U_i^{(\alpha)}} = \frac{1}{2}\int\sum_{p,q}\sum_{\alpha}C_{pqrs}P_{rsk}^{(\alpha)}\left(\sigma_{pq}^{c} - \sigma_{pq}^{s}\right)dV = 0 \tag{B.9}$$

$$\frac{\partial\mathcal{E}'}{\partial\Theta_1^{(\alpha)}} = \frac{1}{2}\int\zeta\sum_{p,q}\sum_{\alpha}C_{pqrs}P_{rs2}^{(\alpha)}\left(\sigma_{pq}^{c} - \sigma_{pq}^{s}\right)dV = 0 \tag{B.10}$$

$$\frac{\partial\mathcal{E}'}{\partial\Theta_2^{(\alpha)}} = \frac{1}{2}\int\zeta\sum_{p,q}\sum_{\alpha}C_{pqrs}P_{rs1}^{(\alpha)}\left(\sigma_{pq}^{c} - \sigma_{pq}^{s}\right)dV = 0 \tag{B.11}$$

Rearranging Eq.(B.9), (B.10) and (B.11) according to the unknown values, we can obtain a matrix equation for the unknown values.

We can also define another error function $\mathcal{E}''$ with stress tensor σ and displacement vector $\mathbf{u}$,

$$\mathcal{E}'' = \int\frac{|\sigma^c - \sigma^s|^2}{|\sigma^c|^2}\mathrm{d}V + \int\frac{|\mathbf{u}^c - \mathbf{u}^s|^2}{|\mathbf{u}^c|^2}\,\mathrm{d}V. \tag{B.12}$$

Appendix C

Rotation Matrix for MSM

$\mathbf{R}_1(\theta)$ is a rotation matrix which rotates vectors by an angle θ about the z-axis in Cartesian coordinate,.

$$\mathbf{R}_1(\theta) = \begin{bmatrix} \cos\theta & -\sin\theta & 0 \\ \sin\theta & \cos\theta & 0 \\ 0 & 0 & 1 \end{bmatrix} \tag{C.1}$$

$\mathbf{R}_2(\theta, \phi)$ is a rotation matrix rotates vectors by an angle ϕ about the normal vector $\mathbf{p}$ $(= \{-\sin\theta, \cos\theta, 0\}^T)$. Using Rodrigues' rotation formula, $\mathbf{R}_2(\theta, \phi)$ can be written as below.

$$\mathbf{R}_2(\theta, \phi) = \begin{bmatrix} (1-\cos\phi)p_1^2 + \cos\phi & (1-\cos\phi)p_1p_2 - p_3\sin\phi & p_2\sin\phi + (1-\cos\phi)p_1p_3 \\ (1-\cos\phi)p_1p_2 + p_3\sin\phi & (1-\cos\phi)p_2^2 + \cos\phi & (1-\cos\phi)p_2p_3 - p_1\sin\phi \\ (1-\cos\phi)p_1p_3 - p_2\sin\phi & p_1\sin\phi + (1-\cos\phi)p_2p_3 & (1-\cos\phi)p_3^2 + \cos\phi \end{bmatrix} \tag{C.2}$$

Appendix D

Shear strength of 2D MSM

In 2D MSM, shear strength, τ_f, is calculated by Mohr–Coulomb failure criterion as follows,

$$\tau_f = \frac{\sigma_3 + \sigma_1}{2} \sin\phi_f = \frac{\sigma_z + \sigma_x}{2} \sin\phi_f \ (\because \text{ plain strain state}) \tag{D.1}$$

And stress tensor, σ, is calculated as summation of mean stress tensor, σ_m, and deviation stress tensor, $\mathbf{s}$.

$$\sigma = \sigma_m + \mathbf{s} = \sigma_m \begin{bmatrix} 1 & 0 \\ 0 & 1 \end{bmatrix} + \int_0^{2\pi} f(\gamma) \begin{bmatrix} -\cos\psi \sin\psi & \cos^2\psi \\ -\cos^2\psi & \cos\psi \sin\psi \end{bmatrix} \mathrm{d}\psi \tag{D.2}$$

therefore, τ_f is a function of mean stress and doesn't change along with shear deforamtion

$$\tau_f = \frac{\sigma_z + \sigma_x}{2} \sin\phi_f = \sigma_m \sin\phi_f \tag{D.3}$$

Bibliography

[1] J. A. Abell, N. Orbović, D. B. McCallen, and B. Jeremic, "Earthquake soil-structure interaction of nuclear power plants, differences in response to 3-d, 3 × 1-d, and 1-d excitations," *Earthquake Engineering and Structural Dynamics*, vol. 47, no. 6, pp. 1478–1495, 2016.

[2] S. Akioka and Y. Muraoka, "Hpc benchmarks on amazon ec2," in *2010 IEEE 24th International Conference on Advanced Information Networking and Applications Workshops*, April 2010, pp. 1029–1034.

[3] P. Amestoy, I. Duff, J. L'Excellent, and J. Koster, "A fully asynchronous multifrontal solver using distributed dynamic scheduling," *SIAM Journal on Matrix Analysis and Applications*, vol. 23, no. 1, pp. 15–41, 2001.

[4] P. R. Amestoy, A. Guermouche, J.-Y. L'Excellent, and S. Pralet, "Hybrid scheduling for the parallel solution of linear systems," *Parallel Computing*, vol. 32, no. 2, pp. 136 – 156, 2006, parallel Matrix Algorithms and Applications (PMAA'04). [Online]. Available: http://www.sciencedirect.com/science/article/pii/S0167819105001328

[5] "Amazon EC2," 2018. [Online]. Available: https://aws.amazon.com/

[6] "Microsoft Azure," 2018. [Online]. Available: https://azure.microsoft.com/

[7] Y. Cai, P. Gould, and C. Desai, "Nonlinear analysis of 3d seismic interaction of soil–pile–structure systems and application," *Engineering Structures*, vol. 22, no. 2, pp. 191 – 199, 2000.

[8] E. N. Dvorkin and K.-J. Bathe, "A continuum mechanics based four node shell element for general non-linear analysis," *Engineering Computations*, vol. 1, no. 1, pp. 77–88, 1984.

[9] "Summary of examination for 14 years by flip research committee, case-example part (in japanese)„" 2011.

[10] "Summary of examination for 14 years by flip research committee, theory part (in japanese)„" 2011.

[11] "Flip consortium," 2018. [Online]. Available: http://www.flip.or.jp

[12] K. Fujita, K. Katsushima, T. Ichimura, M. Horikoshi, K. Nakajima, M. Hori, and L. Maddegedara, "Wave propagation simulation of complex multi-material problems with fast low-order unstructured finite-element meshing and analysis," in *Proceedings of the International Conference on High Performance Computing in Asia-Pacific Region*, ser. HPC Asia 2018. New York, NY, USA: ACM, 2018, pp. 24–35. [Online]. Available: http://doi.acm.org/10.1145/3149457.3149474

[13] A. Fukutake, O. Yasuhiro, K. Nakamura, K. Katsusawa, and S. Yasuo, "building - pile - study of modeling of effective stress analysis of ground system: Effect of comparison and pile volume considering its 3-dimensional analysis and two-dimensional analysis," *Summaries of technical papers of annual meeting*, vol. 2, pp. 465–466, 1996.

[14] "3d geological analysis technology consortium." [Online]. Available: https://www.3dgeoteccon.com/index.html

[15] "GeoFEAS." [Online]. Available: http://www.forum8.co.jp/index.html

[16] "GTS NX." [Online]. Available: http://jp.midasuser.com/geotech/

[17] *Guideline about ensuring reliability of a simulation: The atomic Energy Society of Japan standard*. Atomic Energy Society of Japan, 2016.

[18] A. Gupta, P. Faraboschi, F. Gioachin, L. V. Kale, R. Kaufmann, B. Lee, V. March, D. Milojicic, and C. H. Suen, "Evaluating and improving the performance and scheduling of hpc applications in cloud," *IEEE Transactions on Cloud Computing*, vol. 4, no. 3, pp. 307–321, July 2016.

[19] M. Harada, H. Motegi, H. Gonnokami, and A. Yamaya, "Verification of seismic performance of in-ground lng tank using 3d tank-soil coupled nonlinear fem analysis," *Journal of Japan Society of Civil Engineers*, vol. 67, no. 3, pp. 565–582, 2011.

[20] K. Hijikata, R. Kikuchi, Y. Nukui, A. Imamura, F. Yagishita, T. Mase, H. Yoshida, T. Shiomi, K. Koyamada, and K. Yoshida, "Three dimensional response behavior of unit no.5 reactor building subjected to the niigataken chuetsu-oki earthquake in 2007," *Journal of Structural and Construction Engineering*, vol. 75, no. 658, pp. 2179–2187, 2010.

[21] K. Hijikata, R. Kikuchi, Y. NUKUI, A. IMAMURA, F. YAGISHITA, T. MASE, H. YOSHIDA, K. YOSHIDA, K. KOYAMADA, and T. SHIOMI, "Dynamic response of unit no.7 reactor building during the niigataken chuetsu-oki earthquake in 2007," *Journal of Structural and Construction Engineering*, vol. 76, no. 660, pp. 319–327, 2011.

[22] M. Hori, L. Wijerathne, T. Ichimura, and S. Tanaka, "Meta-modeling for constructing model consistent with continuum mechanics," *Journal of JSCE*, vol. 2, no. 1, pp. 269–275, 2014.

[23] S. Iai, "Micromechanical background to a strain space multiple mechanism model for sand," *SOILS AND FOUNDATIONS*, vol. 33, no. 1, pp. 102–117, 1993.

[24] S. Iai and O. Ozutsumi, "Yield and cyclic behaviour of a strain space multiple mechanism model for granular materials," *International Journal for Numerical and Analytical Methods in Geomechanics*, vol. 29, no. 4, pp. 417–442, 2005.

[25] T. Ichimura, K. Fujita, S. Tanaka, M. Hori, M. Lalith, Y. Shizawa, and H. Kobayashi, "Physics-based urban earthquake simulation enhanced by 10.7 blndof × 30 k time-step unstructured fe non-linear seismic wave simulation," in *SC '14: Proceedings of the International Conference for High Performance Computing, Networking, Storage and Analysis*, Nov 2014, pp. 15–26.

[26] J.JAYASINGHE, S. Tanaka, L. Wijerathne, M. Hori, and T. Ichimura, "Rigorous conversion of solid and beam element solu-tions based on meta-modeling," *Journal of Japan Society of Civil Engineers, Ser. A2*, vol. 70, no. 2, pp. 223–233, 2014.

[27] I. Karunarathna, L. Wijerathne, M. Hori, and T. Ichimura, "Formulation of unified models for beam and shell based on meta-modeling theory," *Journal of Japan Society of Civil Engineers, Ser. A2*, vol. 72, no. 2, pp. 109–119, 2016.

[28] Y. Kim and S. Jeong, "Analysis of soil resistance on laterally loaded piles based on 3d soil and pile interaction," *Computers and Geotechnics*, vol. 38, no. 2, pp. 248 – 257, 2011.

[29] K. Maruyama, M. Horie, and T. Kanazu, "Outlines of guideline and recommendation for seismic performance verification of underground reinforced concrete structures in nuclear power stations and its revised contents," *Concrete Journal*, vol. 43, no. 4, pp. 3–10, 2005.

[30] H. Matsuoka, "Stress-strain relationships of sands based on the mobilized plane," *SOILS AND FOUNDATIONS*, vol. 14, no. 2, pp. 47–61, 1974.

[31] H. Matsuoka and T. Nakai, "Idea and use of compounded mobilized plane and spatially mobilized plane of soil," *Soil and Base*, vol. 33, no. 4, pp. 15–23, 4 1985. [Online]. Available: https://ci.nii.ac.jp/naid/110003966905/

[32] V. Mauch, M. Kunze, and M. Hillenbrand, "High performance cloud computing," *Future Generation Computer Systems*, vol. 29, no. 6, pp. 1408 – 1416, 2013.

[33] P. Mell, T. Grance, *et al.*, "The nist definition of cloud computing," *National institute of standards and technology*, vol. 53, no. 6, p. 50, 2009.

[34] R. D. Mindlin, "Influence of rotatory inertia and shear on flexural motions of isotropic, elastic plates," *J. Appl. Mech.*, vol. 18, pp. 31–38, 1951.

[35] T. Morita, S. Iai, and L. Hanlong, "Parameter setting method for liquefaction analysis program, flip," THE PORT AND HARBOUR RESEARCH INSTITUTE MINISTRY OF TRANSPORT. JAPAN, Tech. Rep. 869, 6 1997.

[36] H. Nagino, A. Shiga, T. Adachi, T. Mizusawa, and T. Mikami, "Ranges in application of classical theory and mindlin theory for bending problem of rectangular plate under surface force on elastic foundation," *Journal of Japan Society of Civil Engineers, Ser. A2*, vol. 70, no. 2, pp. 13–24, 2014.

[37] S. Nishimura and I. Towhata, "A three-dimensional stress-strain model of sand undergoing cyclic rotation of principal stress axes," *SOILS AND FOUNDATIONS*, vol. 44, no. 2, pp. 103–116, 2004.

[38] "PLAXIS 3D." [Online]. Available: https://www.plaxis.com/

[39] E. Roloff, M. Diener, A. Carissimi, and P. O. A. Navaux, "High performance computing in the cloud: Deployment, performance and cost efficiency," in *4th IEEE International Conference on Cloud Computing Technology and Science Proceedings*, Dec 2012, pp. 371–378.

[40] "Soil plus." [Online]. Available: http://www.engineering-eye.com/SOILPLUS/

[41] S.P.Timoshenko, "On the transverse vibrations of bars of uniform cross-section," *The London, Edinburgh, and Dublin Philosophical Magazine and Journal of Science*, vol. 43, no. 253, pp. 125–131, 1922.

[42] M. Takeshi, T. Satoshi, W. Tadatomo, and M. Koichi, "Seismic response analysis of rc pile foundation-soil coupled system using 3d nonlinear finite element method," *Journal of Japan Society of Civil Engineers*, vol. 64, no. 2, pp. 192–207, 2008.

[43] S. Timoshenko and S. Woinowsky-Krieger, *Theory of plates and shells*, ser. Engineering societies monographs. McGraw-Hill, 1959.

[44] I. Towhata, "Modeling soil behaviour under principal stress axes rotation," *Proceedings of 5th International Conference on Numerical Methods in Geomechanics, Nagoya, 1985*, vol. 1, pp. 523–530, 1985.

[45] S. Tsuchiya, N. Chijiwa, M. Harada, T. Mishima, and K. Maekawa, "3d nonlinear finite element seismic analyses of in-ground lng tanks and surrounding soil," *Journal of Japan Society of Civil Engineers*, vol. 71, no. 3, pp. 429–448, 2015.

[46] K. Ueda and S. Iai, "Revisit of the formulation of elastic body considering inherent anisotropy based on the concept of multiple shear mechanism," *Annuals, Disaster Prevention Research Institute, Kyoto University*, no. 59B, pp. 115–124, 2016.

[47] L. Wijerathne, X. Wei, M. Hori, T. Ichimura, and S. Tanaka, "Automated meta-modeling of pipeline network for seismic performance analysis," *Journal of Japan Society of Civil Engineers, Ser. A2*, vol. 70, no. 2, pp. 587–594, 2014.

[48] T. Yamada, T. Ichimura, M. Hori, H. Dobashi, and N. Ohbo, "Evaluation of seismic performance of ramp tunnel structure during level-2 earthquake by massive 3d numerical computation," *Journal of Japan Society of Civil Engineers, Ser. A1*, vol. 68, no. 4, pp. 830–843, 2012.

[49] T. Yamashita, M. Hori, K. Oguni, S. Okazawa, T. Maki, and Y. Takahashi, "Reformulation of non-linear constitutive relations of concrete for large-scale finite element method analysis," *Journal of Japan Society of Civil Engineers, Ser. A2*, vol. 67, no. 1, pp. 145–154, 2011.

[50] Y. Yoshimi and K. Fukutake, *Physical and evaluation measures technology of liquefaction*. Gihodou, 2005.

[51] S. Yoshimura, M. Hori, and M. Ohsaki, *High-Performance Computing for Structural Mechanics and Earthquake Tsunami Engineering*, 1st ed. Springer Publishing Company, Incorporated, 2015.

[52] O. Zienkiewicz, R. Taylor, and J. Zhu, *The Finite Element Method: Its Basis and Fundamentals*, ser. The Finite Element Method. Elsevier Science, 2013.